GL01132

DEPARTMENT OF GEOLOGY AND GEOPHYSICS

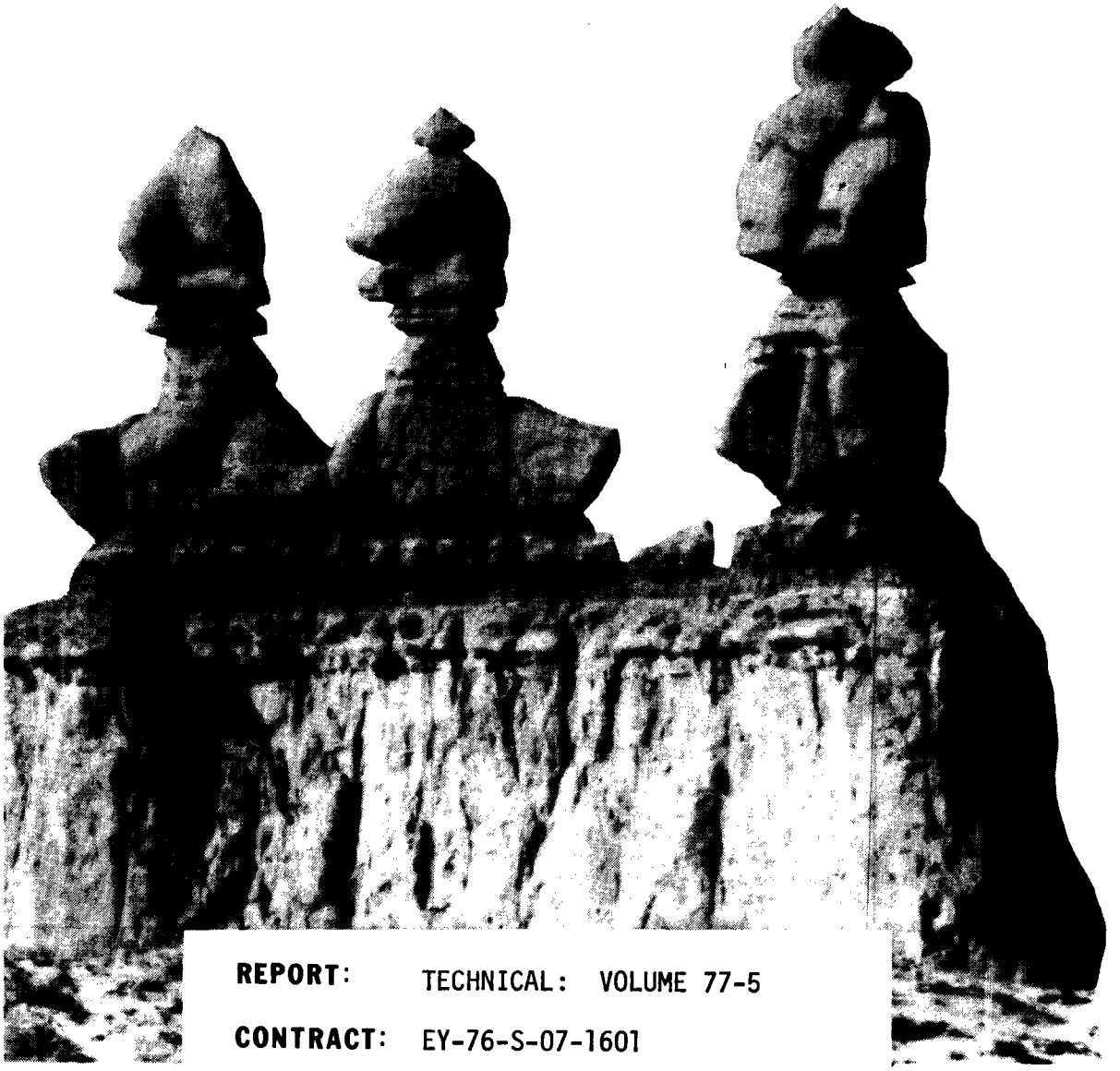

REPORT: TECHNICAL: VOLUME 77-5

CONTRACT: EY-76-S-07-1601

AGENCY: ERDA

TITLE: HYDROTHERMAL ALTERATION AT ROOSEVELT HOT SPRINGS KGRA - DDH 1976-1

AUTHORS: Nancy Lee Bryant and W. T. Parry

DATE: September, 1977

UNIVERSITY OF UTAH SALT LAKE CITY, UTAH 84112

TECHNICAL REPORT: VOLUME 77-5

Hydrothermal Alteration at Roosevelt Hot Springs KGRA - DDH 1976-1

Energy Research and Development Administration

Contract EY-76-S-07-1601

Nancy Lee Bryant

and

W. T. Parry

TABLE OF CONTENTS

Table of Contents (Continued)

LIST OF FIGURES

LIST OF TABLES

ABSTRACT

Hot waters of the Roosevelt Thermal Area, Utah, have altered granitic rocks and detritus of the Mineral Range pluton, Utah. Alteration and mineral deposition recognized in a 200' drill core from DDH 1-76 is most intense in the upper 100 feet which consists of altered alluvium and opal deposits; the lower 100 feet is weakly altered quartz monzonite. Petrographic, X-ray, and chemical methods were used to characterize systematic changes in chemistry and mineralogy.

Major alteration zones include: 1) an advanced argillic zone in the upper 30 feet of altered detritus containing alunite, opal, vermiculite, and relic quartz; 2) an argillic zone from 30 feet to 105 feet containing kaolinite, muscovite, and minor alunite; and 3) a propylitic zone from 105 to 200 feet containing muscovite, pyrite, marcasite, montmorillonite, and chlorite in weakly altered quartz monzonite.

Comparison of the alteration mineral assemblages with known water chemistry and equilibrium activity diagrams suggests that a simple solution equilibrium model cannot account for the alteration. A model is proposed in which upward moving thermal water super-saturated with respect to quartz and a downward moving cool water undersaturated with respect to quartz produces the observed alteration.

An estimate of the heat flow contributions from hydrothermal alteration was made by calculating reaction enthalpies for alteration reactions at each depth. In calculating heat flow, the uncertain variables included: 1) depth of alteration, 2) duration of hydrothermal activity, 3) thermal gradient, and 4) amount of sulfide oxidized to sulfate. The estimated heat flow varied from .02 HFU (for 200' depth, 400,000 yr duration, and no sulfur oxidation) to 67 HFU (for 5,000' depth, 1,000 yr duration, and all sulfur oxidized from sulfide). Heat flow contributions from hydrothermal alteration are comparable with those from a cooling granitic magma.

ACKNOWLEDGEMENTS

Dr. Myron Best of Brigham Young University provided working space and instruction in his laboratory for preparation of glass discs used for XRF analysis. Steve Cone of the late Kennecott Exploration, Inc. provided the basis for the MODECALC program and Judy Ballantyne did the computer programming and calculations.

INTRODUCTION

Purpose and Scope

The purpose of this study is to characterize the hydrothermal alteration in one drill core (U of U DDH 1-76) from the Roosevelt Hot Springs Thermal Area and to describe the geochemical environment in an area where the geothermal reservoir fluid leaks to the surface. A further objective is the calculation of the enthalpy of reaction for all alteration reactions and the estimation of the hydrothermal alteration contribution to the total heat flow of the system.

Alteration mineral assemblages have been studied in almost all well-researched geothermal areas such as Wairakei, New Zealand (Steiner, 1953), Broadlands, New Zealand (Mahon and Finlayson, 1972), Steamboat Springs, Nevada (Schoen and White, 1965; Schoen, White, and Hemley, 1974; Sigvaldason and White, 1961; White, 1968), and Yellowstone Park, Wyoming (Honda, 1970; Rahmahashay, 1968).

Alteration at Steamboat Springs, Nevada, occurs in granodiorite and andesites (Thompson and White, 1962). Only in the Silica Pit area (hole GS-7) does abundant alunite occur below a zone of opaline sinter and cristobalite (Schoen, White, and Hemley, 1974; Sigvaldason and White, 1962) which then grades into a zone containing abundant montmorillonite and kaolinite. Elsewhere at Steamboat Springs, argillic alteration is characterized mainly by kaolinite and variously proportioned illite-montmorillonite (Schoen and White, 1965; Sigvaldason

and White, 1961); propylitic alteration is characterized by chlorite, calcite, and illite (Sigvaldason and White, 1961); sericitic alteration includes illite, quartz and pyrite (Schoen and White, 1965).

The Ohaki-Broadlands Area, described by Browne and Ellis (1970), exhibits alteration in surficial rhyolitic volcanics and buried argillaceous sediments. The altering fluids here are dilute chloride-bicarbonate waters and therefore differ from those at Roosevelt Hot Springs. There is no alunite, very little kaolinite, major amounts of variously proportioned illite-montmorillonite (illite component increasing with depth), pyrite, and calcite with large amounts of chlorite and small amounts of epidote.

In contrast, waters from the Wairakei geothermal area in New Zealand, described by Steiner (1953), have much more sodium chloride and much less bicarbonate than waters from Ohaki-Broadlands. Rhyolite is the major host rock. A surficial acid-leached zone containing kaolinite is followed by an argillic zone containing montmorillonite. These zones are followed at increasing depths by zones of zeolitization and feldspathization.

In the Paint Pot Hill Area, Yellowstone Park, Wyoming (Rahmahashay, 1968), the surficial alteration of alunite and kaolinite resulted from acid waters reacting primarily with a feldspar and quartz host rock. The formation of montmorillonite occurred in a more alkaline environment.

A somewhat different geology of Cenozoic sediments (quartz + plagioclase + K-spar + carbonates + kaolinite + montmorillonite) exists at the Salton Sea Geothermal Area (White and Muffler, 1964).

Two major alteration minerals at depth in drill hole 5232-IID#1 are chlorite (from kaolinite and dolomite) and epidote (from calcite).

Hydrothermal alteration in ore-forming systems typically produces some variation on the scheme: Vein → advanced argillic (kaolinite, alunite, sericite, quartz) → sericitic (sericite, quartz, pyrite) → intermediate argillic (kaolinite, montmorillonite) → propylitic (chlorite, carbonate, montmorillonite) → fresh rock (Meyer and Hemley, 1967). A situation similar to that at Roosevelt Hot Springs (below 110') involves the sericitization of clays and microcline along with the conversion of biotite to sericite and pyrite as seen at Butte, Montana (Meyer and Hemley, 1959).

As exploration tools and means of resource characterization, geochemical analysis of surface and subsurface water and rock are useful.

Location

During the summer of 1976, University of Utah (U of U) alteration hole 1-76 (DDH 1-76) was drilled at the Roosevelt Hot Springs Known Geothermal Resource Area (KGRA), located approximately 13 miles northeast of the town of Milford in Beaver County, Utah. DH 1-76 has a map location of NE 1/4, SW 1/4, Sec. 34, T 26S, R 9W and U of U coordinates of 562ON, 600E (Fig. 1).

Figure 1. Map of Utah showing location of Roosevelt Hot Springs KGRA and geologic map of the Roosevelt Hot Springs KGRA.

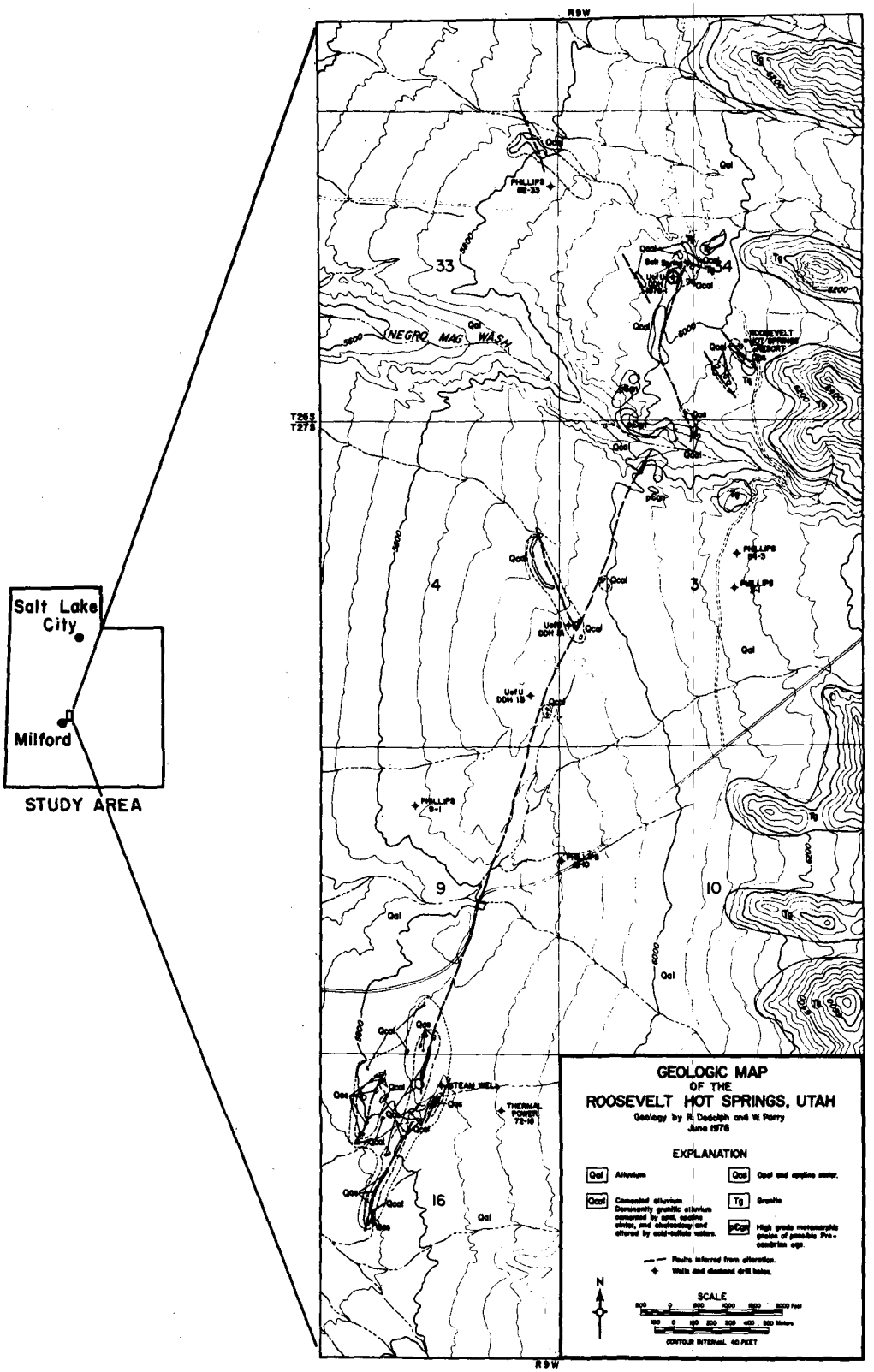
Salt Lake City
Milford
STUDY AREA
R9W
T26S
T27S
NEGRO MAG WASH
ROOSEVELT HOT SPRINGS KGRA
PHILLIPS 86-33
PHILLIPS 84-3
PHILLIPS 9-1
PHILLIPS 24-10
STEAM WELLS
THERMAL POWER 72-16
33
34
4
3
9
10
16
GEOLOGIC MAP
OF THE
ROOSEVELT HOT SPRINGS, UTAH
Geology by R. Dodolph and W. Parry
June 1978
EXPLANATION
Qal Alluvium
Qcal Cemented alluvium. Dominantly granitic alluvium cemented by opal, opaline silica, and chalcedony and altered by acid-sulfate waters.
Qos Opal and opaline sinter.
Tg Granite
pCgr High grade metamorphic gneiss of possible Pre-cambrian age.
Faults inferred from alteration.
Wells and diamond drill holes.
N
SCALE
CONTOUR INTERVAL 40 FEET

mapped, the Dome Fault is the most conspicuous of a set of NE trending faults. Referral to Fig 1 indicates that the opal-cemented alluvium and opal sinter occur not only along this fault, but also along inferred NW trending faults. Fig 2 (Ward and Sill, 1976) indicates faults as interpreted by geological and geophysical techniques.

The study of gravity at the Roosevelt Hot Springs Area by Crebs (1976) indicated that Negro Mag Wash is a fault-controlled stream valley. The fault along this feature has a vertical displacement of 70 m, downthrown on the south. Gravity measurements also indicate that the Dome Fault has formed a horst (Dome Horst) with a 50 m throw. Ward and Sill (1976) interpreted aeromagnetic data as indicating Precambrian bedrock west of the Dome Fault and granitic bedrock to the east of the Dome Fault. The under-lying quartz-monzonite in DDH 1-76 suggests that DDH 1-76 lies on the downthrown side of the Dome Fault (extended to North) and the up-thrown side of the Negro Mag Wash fault. These faults have been the conduits for silica-rich acid-sulfate waters which have risen to the surface depositing SiO_2 in the form of X-ray amorphous opal, α-cristobalite, and micro-crystalline α-quartz and often altering the surface alluvium to alunite. Native sulfur also occurs with alunite and opal. In the area of the Opal Dome (S.W. corner of Figure 1) the deposits consist of "banded and laminated opal" (Parry et al., 1976, p. 23). The colors very widely and range from red, to pink, grey, brown, and green. Though these spring deposits are the most extensive, other opal deposits exist elsewhere along the Dome Fault.

GEOLOGY

Mineral Range Geology

The Mineral Range includes Paleozoic and Mesozoic sedimentary rocks, basalt flows, and metamorphic rocks, but the dominant rocks are the granitic pluton, associated dikes, and younger silicic volcanics that overlie the pluton. Mineral Range geology has been previously summarized (Butler et al., 1920; Earll, 1957; Leise, 1957) and is currently summarized by Evans (1977).

The Mineral Range pluton, 32 km in length by 8 km in width, ranges compositionally from a friable and very weathered granite, to a quartz monzonite, to a cliff-forming granodiorite. A complete petrologic analysis of the pluton has been described by Bowers (1977) who suggests a trend to less acid compositions toward the west.

Armstrong (1970) dated biotite from the west side of the pluton at 9.2±0.3 m.y. Uplift and erosion of the pluton followed, supplying several hundred feet of alluvium to the Milford Valley. Pleistocene basalt flows and rhyolite volcanic eruptions spanned a period of at least 200,000 years (Lipman, et al., 1976). Detailed petrology of these volcanics has been compiled by Nash (1976).

Geology and Structure of the Roosevelt Hot Springs KGRA

The Roosevelt Hot Springs KGRA has been mapped in detail by Petersen (1975) and Parry and Dedolph (1977). Of the surface features

Figure 2. Faulting interpreted from geology, air photos, resistivity, and magnetics for Roosevelt Hot Springs (Ward and Sill, 1976).

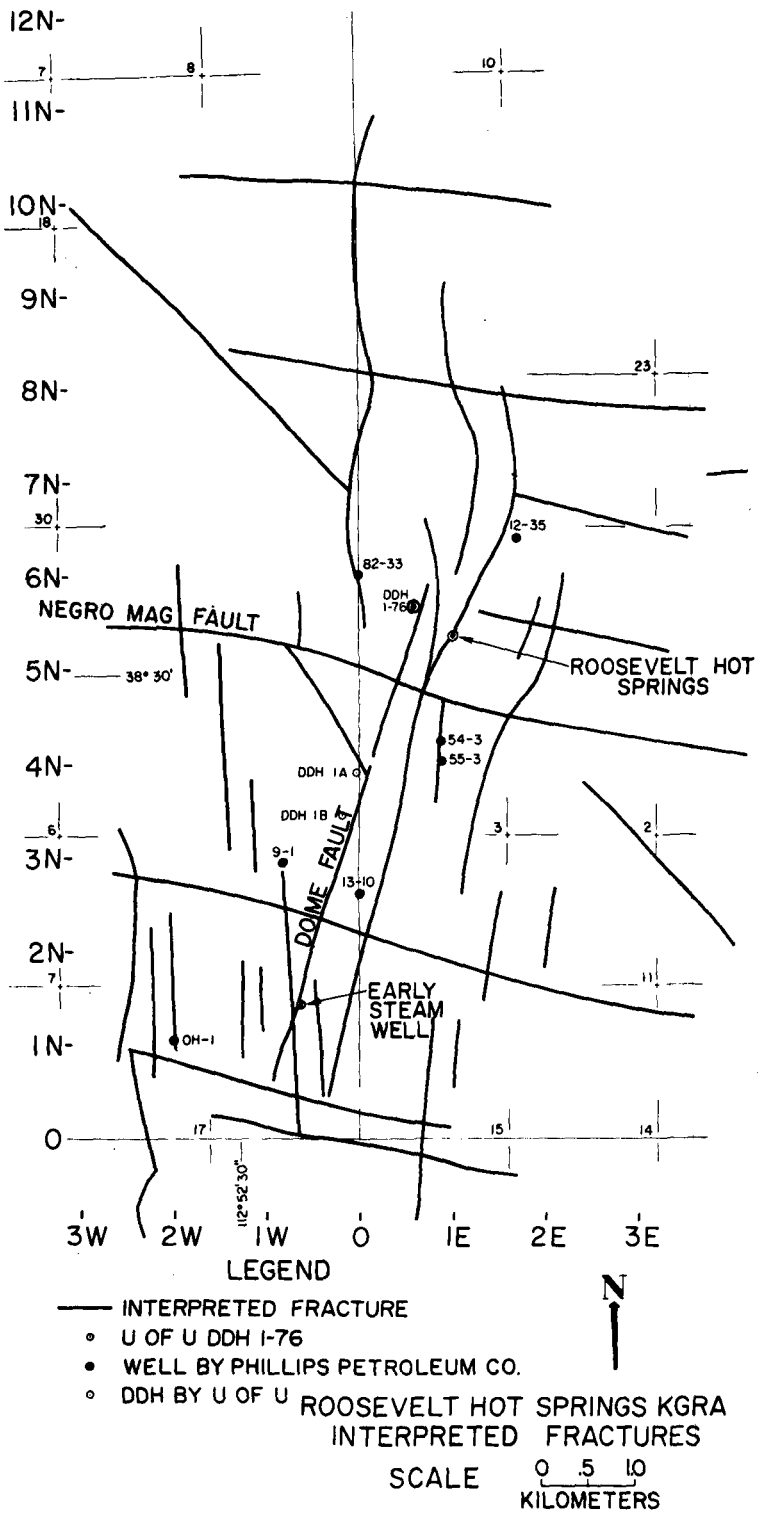
12N-
11N-
10N-
9N-
8N-
7N-
6N-
5N-
4N-
3N-
2N-
1N-
0
38° 30'
112°52'30"
3W
2W
1W
0
1E
2E
3E
NEGRO MAG FAULT
DOME FAULT
ROOSEVELT HOT SPRINGS
82-33
DDH 1-76
12-35
54-3
55-3
DDH 1A
DDH 1B
9-1
13-10
EARLY STEAM WELL
OH-1
LEGEND
INTERPRETED FRACTURE
U OF U DDH 1-76
WELL BY PHILLIPS PETROLEUM CO.
DDH BY U OF U
N
ROOSEVELT HOT SPRINGS KGRA
INTERPRETED FRACTURES
SCALE
0 .5 1.0
KILOMETERS

Subsurface hydrothermal alteration from DDH 1A, previously described by Parry et al. (1976), contains mostly alunite with some sulfur from 0'-70', kaolinite as the major alteration product from 60'-80', abundant montmorillonite with kaolinite and K-mica downward from 80' with K-mica beginning to dominate at 200'.

Water Chemistry

Lee (1908) described the hot springs as having a flow rate of 10 gal/min and a temperature of 190°F (88°C). The springs no longer flowed by 1963 (Mundorff, 1970). There is currently one small seep 500 meters northwest of the early hot spring with a temperature of 25°C.

Chemical analyses of surface waters collected by the USGS in 1957, by the University of Utah research team in 1975, by Phillips Petroleum Co., and by Thermal Power of Utah, are summarized in Table 1.

While there is some variability, the sodium chloride-rich nature of these waters is preserved in all analyses. Ionic strength generally varies from 0.11 to 0.2. Sulfate concentrations vary from 48 to 200 mg/l and total dissolved solids approximate 6000 mg/l. There is a difference between "surface" waters (from the seep; analyses 1 and 2) and the deep waters (analyses 3, 4, and 5). Surface Mg^{2+} increases by a factor of 100, and surface Ca^{2+} increases by a factor of 10 over the deep waters. These ions have been leached from Mg and Ca minerals and are reflected in surface water chemistry.

The warmest Na-K-Ca temperature in the state of Utah (according

Table 1. Selected Roosevelt KGRA Water Analyses

	(1)	(2)	(3)	(4)	(5)	(6)
Na	1840	1800	2400	2000	2072	2500
Ca	122	107	9	10.1	31	22
K	274	280	565	410	403	488
SiO_2	173	107	775	560+	639	313
Mg	25	24	19	.24	.26	0
Cl	3210	3200	4800	3400	3532	4240
SO_4	120	70	200	54	48	73
HCO_3	298	300		200	25	156
S	<.03					
Al					1.86	.04
Fe					.016	-
Total Dissolved Solids		5948		6442		7800
Temp.	25°C	28°C		+260°C	92°C	55°C
pH	6.5	6.43	6.5	6.3	5.0	7.9
Na-K-Ca Temp. Estimate	241	239		294+		

(1) Roosevelt Seep. University of Utah 6-25-75

(2) Roosevelt Seep. Phillips Petroleum Co. 8-15-75

(3) Phillips Well 54-3, Chemical and Mineralogical Services

(4) Phillips Well 54-3, Phillips Petroleum Co. 8-26-75

(5) Thermal Power of Utah 72-16. 1-29-77 Analyses by University of Utah

(6) Roosevelt Hot Springs USGS. Mundorff (1970). Collected 9-11-57

to analysis by Mundorff, 1970; Swanberg, 1974) occurs at Roosevelt Hot Springs. University of Utah analysis of a cool seep indicates a Na-K-Ca wall rock equilibration temperature of 241°C.

In his discussion of thermal waters associated with Tertiary and Quaternary volcanism, White (1957) described waters that are variously enriched with sodium chloride, H^+, sulfate, and bicarbonate. Within White's definitions, Roosevelt Hot Spring's water could be defined as a sodium chloride water grading into an acid sulfate water. The sulfate measurements of 54-200 ppm (at Roosevelt) are lower than those at Norris Basin, Yellowstone Park (454 ppm) or Frying Pan Lake, New Zealand (262 ppm) which have been defined as acid-sulfate, chloride waters. Both Na and Cl contents of waters from Roosevelt are considerably higher than for sodium chloride waters described by White (Steamboat Springs, Washoe County, Nevada; Morgan Springs, Tehama County, California; Norris Basin, Yellowstone Park, Wyoming; Well 4, Wairakei, New Zealand). White envisions these waters having formed by a process which includes: 1) the rising from a magma chamber at depth, of supercritical, high density gases (CO_2, H_2S, alkali halides, SiO_2, etc.); 2) condensation of this phase into a sodium chloride water which heats meteoric water by conduction; 3) the ascension of meteoric water which cools and becomes more acidic as boiling occurs; and 4) the oxidation of H_2S above the water table by atmospheric oxygen. This is not an unreasonable process for the Roosevelt Hot Springs convective hydrothermal system.

Age of Geothermal Activity

Ten K-Ar dates for recent Mineral Range rhyolitic volcanics have

been compiled by Lipman, and others, (1976). The oldest average 2.30 m.y. ± .14 and the younger volcanics range from .42 m.y. ± .07 to .77 m.y. ± .08.

Estimates of the age of surface hot spring activity have been made by Brown (1977a, 1977b), using obsidian hydration rind and paleo-magnetic data. One ring and two half-width hydration bands along cracks were measured (one from Roosevelt seep and two from silicified alluvium) and yielded ages of 220,000, 257,000, and 330,000 years for the development of the rims. Browns' paleomagnetic work attempted to age date the Opal Dome deposits. This work provided much broader limits and less certain dates. The age of the opal is less than 690,000 years (the Brunhes-Matayuma epoch boundary) and greater than 12,000 years (the Laschamp event). Two estimates for opal deposition rates were 1m/5,000 years and 1m/10,000 years which lead to estimates of 70,000 years and 35,000 years for the age of the Opal Dome. If the epoch of the opal deposition activity were correlated, instead, to the Biwa II went, the age of these deposits would be lengthened to 350,000 years.

Heat Source for Geothermal Activity

Igneous activity near the Roosevelt Hot Springs KGRA began with the Tertiary intrusion of the Mineral Range granitic pluton and continued through the Pleistocene rhyolitic volcanics. In his gravity study of the Mineral Mountains, Crebs (1976) identified a north-trending residual gravity low along the volcanic domes of Bearskin, Little Bearskin, North Twin Flat, and South Twin Flat which may possibly indicate a low-density paleo-magma chamber. This fits

nicely into the model proposed by White (1957) which requires a magma chamber for at least some of the chemical species of a hydrothermal fluid and for a means of at least initially heating up the convective system.

Once in motion, however, there are other processes which can continue to warm the hydrothermal fluids: precipitation of solids and wall rock alteration (Toulmin and Clark, 1967). These mechanisms, as they apply to Roosevelt Hot Springs will be discussed later.

CORE ACQUISITION AND DESCRIPTION

During June 1976, Jensen Drilling Co. core-drilled DDH 1-76 using a diamond drill bit. DDH 1-76 is located on a crest of a cemented alluvium ridge north of Negro Mag Wash and west of an inferred fault (heavily-circled locations, Figures 1 and 2).

The core log appears in Table 2 and Figure 3. The upper 110' represent altered granitic alluvium, dominated by alunite, opal, and kaolinite as alteration products. The texture varies from fine-grained clay to coarse-grained altered alluvial pebbles. Unlike U of U DDH 1A, there is no native sulfur present. If the oxidized alunite zone is assumed to be above the water table, then the water table must occur below 105', which corresponds to the driller's estimate. DDH 1A established the water table at 115', which coincides with a fault zone characterized by occasionally abundant pyrite (and marcasite?). Somewhere in this fault zone lies the alluvium-bedrock contact, below which is weakly propylitically and sericitically altered quartz monzonite.

Table 2. Core Log DDH 1-76

Lithology	Depth	Description
GRANITIC ALLUVIUM	10.8'-33.2'	Altered cemented granitic alluvium. Large quartz pebbles and opal patches and veinlets. All feldspars appear altered. Dark brown-gold mica appears at 20'. Staining varies in color from gold to red to pink. Pebble boundaries usually apparent.
	33.2'-60'	Altered opal-cemented granitic alluvium. At 36'-38' there is extensive green colored clay (jarosite?) and hematite and opal. At 42'-43' the core has a homogeneously "baked-grey clay appearance" with fine grains indistinguishable. From 43'-60' some white altered feldspar and quartz pebble outlines are evident. Staining varies between red, black, and gold-colored in a mostly fine-grained matrix. No visible opal at the end of this section.
	60'-75'	At 60', some fresh feldspar grains appear in this granitic alluvium. Extensive hematite staining. Through 65' the texture is large-crumbly grained with abundant green mica. Minerals are altered feldspar and mica along with quartz pebbles. At 70' the core is very hard, pebbles well cemented. Down to 75' alteration appears to increase, and purple staining predominates.
	75'-98'	This section of the core is very fine-grained, apparently still granitic alluvium. Only quartz and opal are identifiable. These clays are mostly blue-grey in color, though toward the bottom of this section, they are also white and flesh-colored. A green clay occurs along fractures.
Water Table	98'-105'	Pyrite appears at 98'. Grain outlines more visible. At 100' the core becomes more crumbly. Appears to be mostly kaolinite cementing quartz.
Fault	105'-117'	At 105' the color changes from white to dark grey-green. Grain size remains coarse until 115', where fault gouge and abundant small pyrite crystals occur. Fault Zone is about

Table 2 (Continued)

Lithology	Depth	Description
		2 feet wide. The alluvium - quartz monzonite contact is somewhere in this zone.
QUARTZ MONZONITE	117'-160'	117'-120' crumbly quartz monzonite with abundant green mica, green, fine-grained clay, pyrite, feldspars, and quartz. Downward from 120' mineralogy is similar in well-consolidated quartz monzonite.
	160'-200'	Same mineralogy and texture persists, at 162'-163' there are some large (0.5cm) fractures filled with green mineral and abundant pyrite. Downward, the granite (monzonite?) is fairly fresh. Biotite shows some alteration. Green mineral along fractures persists.

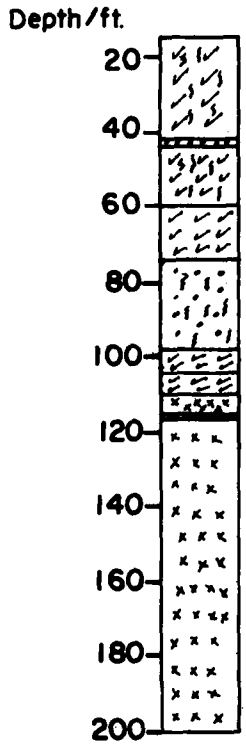

OPAL PATCHES AND VEINLETS THROUGHOUT
GOLD-BROWN MICA. GOLD, RED AND PINK STAINING

EXTENSIVE LIME-GREEN CLAY IN FRACTURE (JAROSITE)
VERY FINE GRAINED GREY CLAY

ALTERED FELDSPAR AND PEBBLE OUTLINES VISIBLE IN FINE GRAINED MATRIX
PEBBLES VISIBLE WITH ABUNDANT GREEN MICA

BLUE-GREY CLAY WITH QUARTZ AND OPAL VISIBLE AND GREEN MICA VISIBLE ALONG FRACTURES

PYRITE APPEARS
WATER TABLE (APPROXIMATE)
APPROXIMATE LOCATION OF ALLUVIUM /QTZ. MONZONITE CONTACT
FAULT

WEAKLY ALTERED QUARTZ MONZONITE
PYRITE THROUGHOUT
GREEN MICA ALONG FRACTURES

ALTERED GRANITIC ALLUVIUM

FINE-GRAINED CLAY

OPAL

QUARTZ MONZONITE

Figure 3. DDH 1-76 Lithologic Core Log.

METHODS

X-ray Fluorescence

Major elements were determined by means of X-ray fluorescence (Phillips Electronic Instruments). The samples were prepared by crushing to 0.25 inch pieces in a small jaw crusher with ceramic plates, followed by pulverizing the sample in a tungsten carbide ball mill (Pitchford Manufacturing PICA MILL). Sulfur analyses were performed on pellets made by mixing one gram of pulverized rock with one gram of chromatographic cellulose (Whatman NO. CF11), pouring into a 1.25 inch diameter aluminum cap (Spex Inc.), and pressing with 20 tons force. The remaining elemental analyses were performed on glass discs following the method of Norrish and Hutton (1969) and modified by Best, Neilson, and Brimhall (1976). 2.25 g of flux (Type 105 of Johnson Matthey Chemical Ltd, containing 47% lithium tetraborate, 37% Li_2CO_3, and 16% lanthanum oxide), 0.03 g of $LiNO_3$ (EM Laboratories Suprapur, CAT. #5653), and 0.42 g of pulverized rock were mixed together and fused into a 1.25 inch diameter disc. The analyzing conditions are listed in Table 3. Loss on ignition values were calculated on separate samples by weighing .4 to .5 g of rock powder into a ceramic crucible, heating at 950° for 15 minutes, followed by re-weighing. These conditions were chosen to approximate those during the fusion process.

A computer program (Appendix 1) was written to apply matrix

Table 3. X-ray Fluorescence Analysis. Analytical Conditions

Element	S	Na	Mg	Al	Si	K	Ca	Fe	Ti
X-ray Tube Target	Cr	Cr	Cr	Cr	Cr	Cr	Cr	W	Cr
Kilovolts	40	40	40	40	40	40	40	40	40
Milliamperes	40	50	40	40	40	40	40	5	40
Analyzing Crystal	EDDT	RAP	RAP	EDDT	EDDT	EDDT	EDDT	LiF200	LiF200
Detector	Flow Counter	Flow Counter	Flow Counter	Flow Counter	Flow Counter	Flow Counter	Flow Counter	Scint.	Flow Counter
Analytical line two theta	75.08	54.32	44.52	142.53	107.92	50.23	44.90	57.55	86.24
Background Line two theta	76.08	55	43	141	109.5	49.0	44	59	88.5
Counting time	10 sec	100 sec	100 sec	20 sec	10 sec	10 sec	10 sec	20 sec	10 sec
Path	VAC	VAC	VAC	VAC	VAC	VAC	VAC	AIR	VAC
Pellet Type	Powder	Glass	Glass	Glass	Glass	Glass	Glass	Glass	Glass

correction factors (Norrish and Hutton, 1969) to initial elemental estimates for analyses on glass pellets, except sodium. Three iterations were made to insure convergence.

Because there were no furnished matrix correction coefficients for sodium, sodium values were not themselves corrected, but were fed into the program to contribute matrix effect corrections for the other elements.

Because SO_2 was lost in the glass pellet-making process, sulfur analyses were made on cellulose pellets. The standards were from the Kennecott Research Laboratories. These analyses were not matrix-corrected, but were input for the XRF DATA REDUCTION PROGRAM to contribute matrix-effect corrections for the other elements.

Microscopic Petrography

Point counts (1,000 points per slide) were made for several thin sections per alteration zone. Mineral abundances and phase relationships were determined by this method.

X-ray Diffraction

X-ray diffraction was used for identification of most whole-rock phases as well as clay minerals. The -2μ size fraction was used on oriented smears for clay determination. Standard clay analytic techniques were used: peptization of clay samples with calgon, vapor glycolation for identification of expandable clays, and heating at 250°C and 500°C for identification of collapsing characteristics.

Mineral Modal Estimates

A computer program, MODECALC, compiled by Ballantyne (1977),

was used to assign mineral abundances to each sample based on mineral identifications made by thin section (Table 6) and X-ray diffraction analyses and on chemical composition determined by XRF (Table 5). The method used is a weighted least squares analysis with an option to weight visually estimated petrographic modes as required. Theoretically, the actual abundance of any element is the sum of the products of each mineral times the number of moles of the element in that mineral.

$$Y(I) = \sum_{J=0}^{N} X(I,J) \times Beta(J)$$

where $Y(I)$ = whole rock analysis of i^{th} element
$X(I,J)$ = j^{th} mineral and i^{th} component
Beta (J) = modal abundance of j^{th} mineral

Linear equations for each element are written with no more minerals than there are number of elemental analyses. Matrix inversion solves for the modal abundance (BETA) matrix. This allows recalculation of elemental abundance, Y'(I), and a computation of goodness of fit:

$$FIT = \sum_{J=0}^{N} W(I) \times (Y'(I)-Y(I))^2$$

where FIT = goodness of fit
$W(I)$ = weighting given to i^{th} elemental analysis

The square of the distance between actual and calculated elemental abundances is minimized.

Mineral compositions used in this program are listed in Table 4. The program does not differentiate between quartz and opal, which is abundantly present in the upper zones. The average SiO_2 content of the alluvium and granite is taken as 66% based on the average SiO_2

Table 4. Mineral Compositions for MODECALC

Mineral	Formula
Quartz	SiO_2
Orthoclase (MR7429)	$K_{.885}Na_{.112}Ca_{.001}Al_{1.006}Si_{2.996}O_8$
Plagioclase (MR7429)	$K_{.025}Na_{.902}Ca_{.073}Al_{1.076}Si_{2.925}O_8$
Biotite (.6 Phlogopite)	$KMg_{1.8}Fe_{1.2}Si_3AlO_{10}(OH)_2$
Muscovite	$KAl_3Si_3O_{10}(OH)_2$
Alunite	$KAl_3(SO_4)_2(OH)_6$
Kaolinite	$Al_2Si_2O_5(OH)_4$
Vermiculite	$Mg_{2.50}Fe_{.5}Al_{.5}Si_{3.5}O_{10}(OH)_2 \cdot 4H_2O$
Montmorillonite	$(Ca_{.04}Na_{.03}K_{.07})(Mg_{.33}Fe_{.09}Al_{1.67})(Si_{3.97}Al_{.03})O_{10}(OH)_2$
Ripidolite	$Ca_{.02}Mg_{2.29}Fe_{1.76}Ti_{.07}Al_{1.09}Si_{2.58}Al_{1.42}O_{10}(OH)_8$
Calcite	$CaCO_3$
Pyrite -Marcasite	FeS_2
Sphene	$CaTi(SiO_5)$
Rutile	TiO_2

composition of DDH 1-76 at depth. All of the titanium above 165' was placed in rutile, which is seen as blood red sphene replacement crystals. Rutile continues to exist below 165' as partial replacement of sphene; however, the titanium was entirely assigned to sphene. The plagioclase and orthoclase compositions are those determined by Evans (1977) on samples from the Mineral Range granite pluton. The composition of Mineral Range biotite was determined by Parry and Jacobs (1976) as having $X_{phlog} = 0.6$. A Mg-rich vermiculite composition was chosen from Nraigu (1975) in order to approximate a reasonable alteration product from a Mineral Range biotite. The montmorillonite composition is an approximate composition as determined by atomic absorption analysis of a purified mineral separate (Appendix 2). The charge deficiency of this clay is only .18, which is too low for an actual montmorillonite (charge deficiency of about .35). Although in obvious error, this analysis was used because it was the only one available. The ripidolite composition (Deer, Howie, and Zussman, 1966) was chosen for its high Mg content to be consistent with the similarly enriched biotite and montmorillonite. Kaolinite, pyrite, muscovite, calcite, sphene, and alunite were assigned stoichiometric compositions.

ALTERATION IN DDH 1-76

Mineralogy has been determined by hand specimen identification, optical methods, and X-ray diffraction. The results of these investigations follow.

The host rocks are dominantly granitic (with perhaps some additions from Precambrian (?) gneiss) alluvium from the Mineral Mountains in the upper 100' of core and quartz monzonite in the lower core. The major minerals include about 15% quartz, 35% plagioclase (An_{12}), 25% orthoclase, and 15% biotite.

Primary Minerals

Quartz. Though not compositionally altered, quartz was subjected to shearing stresses which caused considerable elongation of grains and distortion of normal extinction patterns. Grains were large and anhedral.

X-ray diffraction indicates α-quartz throughout by typical spacings: 4.21Å, 3.33Å, 2.42Å, etc.

Plagioclase. There were only two crystals for suitable plagioclase determination by optical methods. The estimate of An_{12} agrees with other estimates (Bowers, 1977; Evans, 1977). Usually plagioclase cannot be optically distinguished from orthoclase. It often exhibits marked sericitization, except around 65' and in the deepest part of the core.

X-ray diffraction delineated this plagioclase with characteristic albite d spacings of 3.18Å, 5.83Å, and 6.33Å. XRD indicates plagioclase (albite) at depths: 70', 75', and downward from 120'.

Microcline. Microcline appears in thin section downward from 30'. Only a few percent of the crystals have the typical "gridiron" structure, with the majority showing a vague twinning with wavy extinction. Sericite alteration of microcline is common. A considerable proportion of all feldspars are criss-crossed with opal and clay.

X-ray diffraction also suggests microcline downward from 30' by the characteristic d spacings: 3.21Å, 3.27Å, 3.45Å, 3.75Å and others.

Biotite. Biotite appears downward from 120' although, at that point, it is extensively replaced by K-mica. Elsewhere, partial replacement of biotite by a combination chlorite, calcite, K-mica, pyrite, and iron oxides is common. It is pleochroic from light brown to green.

Sphene. Sphene is recognized optically, but not by X-ray diffraction, downward from 175'. At 175', there are two acute rhombic adjoining sections having titanium dioxide (rutile?) along the cleavage with sphene appearing between cleavage. At 180' there are numerous crystals of sphene with various amount of alteration, apparently to titanium dioxide. In one instance, sphene, along with its alteration product, TiO_2, occurs with quartz, muscovite, calcite, hematite, and chlorite.

Alteration Minerals

Opal. Opal appears in hand specimen from 12' through 42' and

from 75' through 95'. Since opal is an amorphous substance, it has no x-ray diffraction lines. In thin section it is a muddy-brown isotropic substance which occurs as feldspar replacement, fracture filling, and as a surficial precipitate on other minerals.

Cristobalite. In thin section, cristobalite is easily confused with opal in its being fairly isotropic, and with very fine-grained quartz when it is not as isotropic. This is an intermediate recrystallization product from opal.

The identification of cristobalite is made on the basis of diffraction patterns from samples taken at 80', 90' and 100', which show strong peaks at 4.05-4.15Å and at 2.53Å.

α-quartz. Secondary α-quartz, as small crystals, is seen throughout the core, even at depth, in veinlets and in intergranular spaces. It is the final recrystallization product after opal and cristobalite.

Alunite. Alunite is seen microscopically as small rhombs replacing feldspar clasts and filling intergranular and fracture spaces. It also rims blebs of microcrystalline quartz and opal. At 38', green jarosite occurs abundantly.

Characteristic alunite lines appear prominently on X-ray diffraction patterns of samples taken from 12' through 25'. Alunite occurs to 110' in small amounts as suggested by very small peak heights on the X-ray diffraction patterns.

Kaolinite. Kaolinites appears microscopically as very fine-grained low-birefringence masses. It is similar and, perhaps not distinguishable from microcrystalline quartz. From 30' to 105' it replaces

feldspar clasts and also occurs in veinlets, sometimes with opal. It is often rimmed by alunite above 38'. At 38' kaolinite appears with opal and jarosite in a "stringer" arrangement.

X-ray diffraction identifies kaolinite from 25' to 105' by the characteristic d spacings: 7.14Å, 3.47Å, and others.

Rutile. Rutile (or some polymorph) has resulted from alteration of sphene, since the cleavage traces and acute rhombic sections are preserved. This mineral is rust brown in thin section. TiO_2 occurs throughout the core until about 170' where sphene remains mostly unaltered. In the propylitic zones, it has the following occurrences: 1) a core of red translucent iron oxide with titanium dioxide surrounding it and 2) titanium dioxide embayed by green muscovite and surrounded by a very small amount of supposed chlorite. In the lower core, TiO_2 occurs as incipient sphene alteration, and also with hematite in veinlets or in apparent amphibole replacement.

X-ray diffraction gives no evidence for any polymorph of TiO_2.

Muscovite. Muscovite is identified microscopically in two forms: 1) classical sericite as small high-birefringence laths and 2) "green muscovite" as large green laths. Below 38' there are also a few occurrences with altered feldspars, of white mica with the high birefringence of typical sericite. The sericite is seen at 70', 90' and 95' with kaolinite and opal. Sericitization of feldspar occurs downward from 105', varying in extent, but generally decreasing. Below 125' sericite occasionally occurs with microcrystalline quartz in veinlets. "Green muscovite" occurs sparsely above 105', except at 65' where it appears abundantly in replacement of biotite. At 80'

it appears to replace a few amphibole crystals. Below 105' green mica increases in abundance and is often accompanied by pyrite in biotite replacement with an occasional biotite core. At 110' and below 125' "green muscovite" is associated with chlorite and sometimes calcite.

X-ray diffraction indicates K-mica from 120'-200' with the characteristic spacing 9.8Å, 4.8Å, 2.95Å, and others.

Vermiculite. Vermiculite is seen in the core apparently as gold-brown altered biotite. In thin section through the upper 105' it has a vermiform shape and a muddy-buff color which sometimes masks its low birefringence. The crystals are fairly large and sometimes containing flecks of iron oxide. In the 30'-60' zone, vermiculite partially embays feldspar clasts.

There is little evidence in X-ray diffraction to support the optical identification of vermiculite. Since the crystals are mostly larger than 2μ, the clay size separation (even after grinding) may have excluded most all vermiculite crystals. At 70' however, there is some evidence. The air-dried oriented slide shows a broad peak centered approximately at 14Å, which is retained upon glycolation. Heating to 250° results in collapse to 10Å; however there are small 13Å-14Å peaks which suggest, perhaps, partial rehydration.

Pyrite and marcasite. Pyrite is seen in hand specimen downward from 90'. This study has not differentiated between pyrite and marcasite, though marcasite has been confirmed in polished sections as overgrowths on cubic pyrite.

Pyrite is tentatively identified in thin section by its cubic

crystal habit. It occurs with iron oxides in veinlets and also in biotite alteration products.

X-ray diffraction consistently identified pyrite downward from 120' by characteristic d spacings of 2.71Å, 2.42Å (located on the side of a quartz peak), and 3.1Å (located in the side of a strong albite peak).

Montmorillonite. Montmorillonite is suspected, and confused with sericite, in thin section between 105' and 150', due to an obvious presence of high birefringence small laths with incompletely altered feldspars.

X-ray diffraction confirms its presence at 105', 115', and 120' by the characteristic 14Å peak (air dried) which expands to a sharp 17Å peak upon glycolation, and collapses to 10Å upon heating.

Randomly Interstratified Clay. Optical identification of these clays was not possible.

Interstratified clays were identified by X-ray diffraction; their characteristics are as follows: 1) illite-montmorillonite (montmorillonite predominant) at 125' with the air-dried slide having a broad 11-17Å peak which expands to 17-20Å upon glycolation, and then collapses to 10Å at 250°C and 2) illite-montmorillonite (illite predominant) at 130', 135' and 145' with the air-dried slide having a broad 11-14Å peak which sharpens at about 12Å upon glycolation, and collapses to 10Å upon heating to 250°C.

Chlorite. Chlorite appears in thin sections at 120', in very small amounts, as small radiating fibres along with green muscovite, pyrite, and iron oxides in biotite replacement. This identification

is based on its green color and very low birefringence (as distinct from the high birefringence of green K-mica) and an occasional anomalous blue interference color. Chlorite is seen more abundantly (almost always with green muscovite) throughout the rest of the core. At 125', 135', and 155'-165', chlorite occurs with calcite, iron oxides, and sometimes pyrite in replacement of biotite and perhaps amphibole. Feldspar also appears to be replaced by chlorite and sericite as deep as 175'. In all replacement environments, chlorite occurs in both lath-like and fibrous habits.

Chlorite was not confirmed by X-ray diffraction because there is so little of it.

Calcite. All of the carbonate seen in thin section is a light tan color with characteristic very high birefringence. It is not known whether this is actually calcite (as opposed to Mg or Fe-rich carbonates) or not; however, it will be referred to as such. Surprisingly, calcite occurs at 12' along with alunite. It does not appear thereafter until 125'-135', 155'-165', and at 180'. At 125' it is seen in thin section in three different environments. In amphibole replacement, calcite occurs with pyrite, green muscovite, and titanium dioxide. Secondly, there are large blebs consisting of calcite on the interior, rimmed by red iron-oxide, which is in turn sometimes rimmed by an opaque mineral. A third occurrence is in veinlets along with opaques, iron-oxide, and sericite. At 130'-135', calcite occurs in amphibole replacement along with microcrystalline quartz, green muscovite, and possible chlorite. It also occurs as veinlets. In the 155-165' area, in addition to the above listed types

of occurrences, there are the following: 1) rectangular crystal replaced with calcite, green muscovite, red iron-oxide, and pyrite, and 2) along the cleavage of biotite replaced by green muscovite.

Nowhere does X-ray diffraction confirm the presence of calcite.

Whole Rock Chemistry

The results of whole rock analyses by XRF, listed in Table 5, show some systematic variations in the core. Abundant opal and quartz is reflected generally by SiO_2 in excess of 66%. The upper core (above 85') contains an average of 14% Al_2O_3 relative to the most intense kaolinite zone (20%) and also relative to the lower core, 17% Al_2O_3. Ti, Fe, and Mg increase downward as these elements are increasingly fixed in primary sphene and biotite. After a high of 15% above 30', sulfate decreases to less than 1% until it no longer exists at 105'. Thereafter, sulfide persists in pyrite and marcasite, usually less than .3%.

The alkalies Na, K, and Ca reflect the relative strength of the leaching environment. Figure 4 plots percent of K_2O, Na_2O, and CaO with depth. While there is variability in the "smoothness" of each curve, there is general consistency in the shapes of each curve. The generalized alkali curve has low values throughout the upper 60' with a sharp rise to intermediate values at 65'. Somewhere between 100' and 120' there is a rise to high levels which persist to 200' except for a sharp drop to intermediate oxide percent at approximately 162'.

These curves, of course, not only reflect mineral abundances and transitions through various stability fields, but also highlight some

Table 5

Roosevelt Hot Springs DDH 1-76
Major Element Analyses

	12'	15'	20'	25'	30'	35'	38'	40'	45'	50'	55'	60'	65'	70'
SiO_2	69.07	55.11	73.51	59.26	56.57	80.48	73.62	78.70	77.14	76.09	69.39	68.36	67.31	69.77
Al_2O_3	9.64	17.91	10.70	17.42	14.42	13.32	14.07	12.11	14.00	13.77	18.05	16.67	14.96	14.19
TiO_2	0.35	0.36	0.49	0.29	0.31	0.43	0.35	0.30	1.06	0.74	0.67	0.82	0.78	0.76
Fe_2O_3	0.18	0.98	0.75	0.35	0.32	0.28	0.80	0.19	0.80	1.07	1.52	0.58	3.49	1.55
MgO	0.34	0.37	0.33	0.28	0.39	0.36	0.38	0.30	0.41	0.21	0.31	0.28	0.57	0.27
CaO	0.40	0.34	0.34	0.34	0.35	0.34	0.43	0.52	0.45	0.45	0.39	0.44	1.33	0.68
Na_2O	n.d.	n.d.	n.d.	n.d.	n.d.	n.d.	n.d.	n.d.	n.d.	n.d.	n.d.	n.d.	3.58	2.87
K_2O	2.78	3.87	2.25	3.85	4.09	1.53	2.78	2.69	3.36	3.20	3.62	7.04	6.42	8.18
L.O.I.*	4.34	6.60	4.53	4.87	5.89	5.68	7.23	6.43	5.64	5.24	5.43	3.95	0.96	1.68
SO_3	10.22	14.22	8.56	14.72	15.40	0.34	1.90	0.32	0.42	2.07	1.07	0.52	0.08	0.35
S														
S=0														
TOTAL	97.33	99.74	101.52	101.38	97.73	102.76	100.56	101.55	103.28	102.83	100.46	98.66	99.58	100.31

*Loss on Ignition minus sulfur

	75'	80'	85'	90'	95'	100'	105'	110'	115'	120'	125'	130'	135'	140'
SiO_2	76.02	74.75	74.80	69.81	64.81	62.03	59.71	67.00	61.24	64.81	63.28	63.39	63.70	66.09
Al_2O_3	13.87	14.10	14.39	21.79	20.04	20.89	20.02	14.50	16.00	17.12	19.84	16.08	16.93	15.71
TiO_2	0.58	4.12	3.63	0.62	0.94	0.89	1.01	0.61	1.12	0.61	0.60	0.79	0.85	0.68
Fe_2O_3	0.44	2.04	1.83	0.36	0.48	0.85	1.90	0.44	6.84	3.23	3.47	3.20	3.85	3.34
MgO	0.37	0.26	0.29	0.26	0.32	0.43	0.45	0.24	0.74	0.39	0.51	0.66	0.66	0.66
CaO	0.33	0.52	0.52	0.37	0.45	0.59	0.88	0.41	0.68	0.54	0.84	1.51	1.40	1.48
Na_2O	n.d.	n.d.	n.d.	n.d.	n.d.	n.d.	n.d.	n.d.	n.d.	3.37	3.13	3.66	4.02	3.60
K_2O	3.77	0.34	0.40	5.11	1.82	1.58	4.54	12.46	8.34	8.70	7.76	7.22	6.22	6.54
L.O.I.*	4.20	5.23	5.85	4.84	8.40	9.23	4.95	0.44	0.00	0.00	0.00	0.74	1.17	0.90
SO_3	0.51	0.61	0.75	0.46	0.60	0.65								
S						0.06	1.64	0.20	1.96	1.26	0.97	0.22	0.24	0.09
S=0						.03	.82	.10	.98	.63	.48	.11	.12	.04
TOTAL	100.09	101.97	102.46	103.63	97.87	97.92	94.29	96.20	95.95	99.39	99.91	96.63	97.74	98.14

*Loss on Ignition minus sulfur

	145'	150'	155'	160'	162'	165'	170'	175'	180'	185'	190'	195'	200'
SiO_2	68.46	64.05	65.56	65.44	75.08	72.70	66.03	65.80	63.10	62.77	61.61	62.15	63.07
Al_2O_3	14.56	17.89	17.13	19.76	12.72	14.82	15.35	15.61	17.88	17.46	20.06	16.33	16.13
TiO_2	0.55	0.62	0.71	0.63	0.57	0.47	0.65	0.75	0.86	0.80	0.72	0.65	0.79
Fe_2O_3	2.78	3.39	3.16	3.29	2.55	2.37	3.43	3.68	3.67	4.08	3.89	3.43	4.23
MgO	0.54	0.79	0.86	0.48	0.50	0.65	0.66	0.90	1.07	1.10	1.16	1.03	1.31
CaO	1.27	1.61	1.66	1.07	0.58	1.12	1.42	1.87	2.32	2.17	2.25	2.34	2.52
Na_2O	3.60	3.86	3.98	3.11	2.93	3.19	3.94	3.96	3.87	4.15	4.11	3.98	4.11
K_2O	6.60	6.58	6.35	6.83	4.56	5.98	6.42	5.64	6.14	5.77	5.49	6.02	5.56
L.O.I.*	0.67	0.68	0.88	1.03	0.00	0.42	0.29	0.30	0.44	0.82	1.15	0.99	1.18
SO_3													
S	0.06	0.06	0.17	0.17	0.42	0.10	0.07	0.06	0.11	0.16	0.15	0.16	0.14
S=0	.03	.03	.08	.08	.21	.05	.04	.03	.05	.08	.07	.08	.07
TOTAL	98.38	98.83	99.50	100.68	99.70	101.35	97.93	98.23	98.96	98.39	99.36	96.09	97.79

*Loss on Ignition minus sulfur

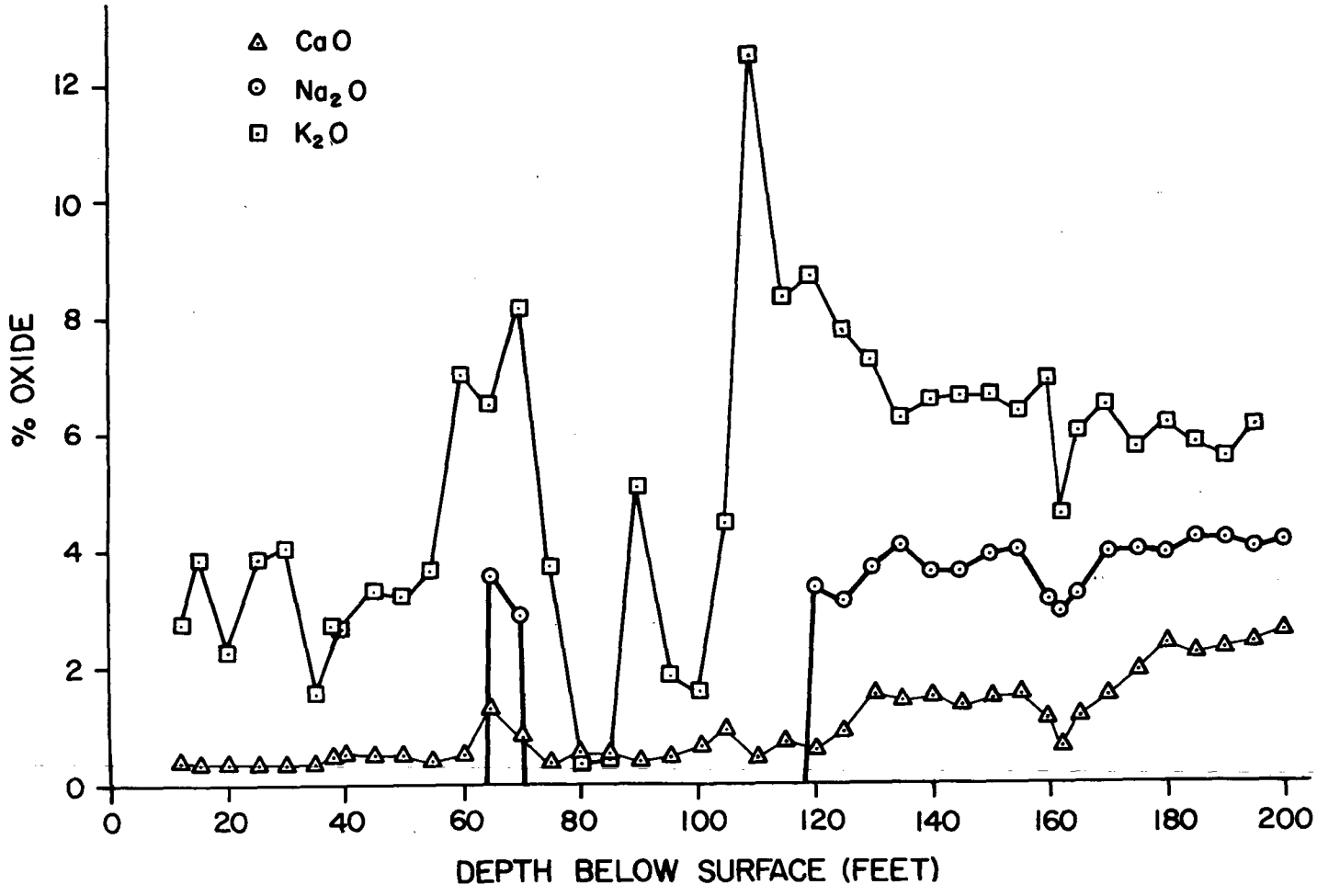

Figure 4. K_2O, Na_2O, and CaO Abundances versus Depth.

fracturing which controls movement of the hydrothermal fluids. Major fracture outlets are seen as relative lows (the surface, 100', and 162') and represent relative lows in pH and alkali. The reaction progress about each fracture is seen in increased alkali content.

Results of Point Counting and MODECALC

Mineralogic abundances were estimated in all samples. Representative thin sections from each zone were point-counted and mineral estimates were also made by the computer routine MODECALC previously described. Point counting results and MODECALC results are listed in Tables 6 and 7. There are several important observations about these tables: 1) point counts distinguish between quartz and opal, while MODECALC does not; 2) point counts distinguish small grains of white mica from very fine-grained sericite (which looks like, and is grouped with montmorillonite in the point counts), and also distinguishes sericite from the green muscovite (both fibrous and platy), while MODECALC categorizes these just as K-mica or montmorillonite; 3) point counts list feldspars as either fresh or altered, while MODECALC differentiates only orthoclase or plagioclase; 4) large amounts of fine-grained groundmass in parts of the upper 115' make point count determinations very uncertain; and 5) although chlorite and calcite terminate at 160' in the MODECALC listing, they actually persist in trace amounts to 200'.

Despite these differences there is generally good agreement between these methods of abundance estimation. Throughout the remainder of this discussion, mineral abundances will be those made by

Table 6. Mineral Abundance Estimates from Thin Section Point Count, in Volume Percent

	Depth												
	12'	25'	35'	38'	60'	65'	80'	95'	110'	120'	135'	165'	190'
Quartz	12	31	18	19	16	19	41	6%	13	19	12	9	20
Vermiculite	3	1	4	4	24	<<1	19	9%					
Opal	35	22	25	37	26	2		5	<1				
Alunite	49	21					<1						
Jarosite				5									
White Mica		1	<1	7									
Groundmass	<<1	24	34				26	59	60				
TiO_2	<1	<1	<1	<1	2	3		1	4	2	2	3	<1
Opaque		<1	1		1	5	<1			3	7	6	6
Kaolinite			5	6	12	<1	12	11					
Altered Feldspar			8	11	4	6		9		44	36	30	3
Fresh Feldspar			3	11	15	42			22	24	34	47	58
Green muscovite						22	1			7	5	3	2
Primary biotite										1	<1	<1	8
Sericite or Montmorillonite						<1	1		1				
Chlorite										<1	2	<1	<1
Sphene													2
Calcite	1											2	1

Table 7. Mineral Abundances as Determined by MODECALC

Depth	Quartz	Plag.	Orth.	Biotite	K-Mica	Alunite	Verm.	Kaol.	Mont.	Chlorite	Calcite	Pyrite	Rutile	Sphene	Total
12'	70					27	2						0.4		99.4
15'	54					41	2						0.4		97.4
20'	72					24	2						0.5		98.5
25'	56				5	37	1						0.3		99.3
30'	52		2			35	2	7					0.3		98.3
35'	60		10		3	0.9	2	22					0.4		98.3
38'	52		13		10	2	2	17					0.3		96.3
40'	57		13		9	0.8	2	15					0.3		97.1
45'	52		16		9	1	3	15					0.9		96.9
50'	54		14		8	4	2	14					0.6		95.6
55'	37		23				1	35				2	0.7		98.7
60'	36	0.2	35			0.6	2	23					0.9		97.7
65'	32	1	38	5	17	0.5	0.4	0.5					0.8		95.2
70'	28	17	40		4	0.5	2	6					0.6		98.1
75'	48	3	23		5	0.6	2	16					0.5		98.1
80'	57				1	2	1	32					4		97.0
85'	55	3	1		2	2	2	26					3		94.0
90'	38		9		28	1	1	21					0.6		98.6
95'	36		10			2	2	48					1		99.0
100'	33		9			2	2	52				0.2	0.9		99.1
105'	26		19		14		2	27	8			3	1		100.0
110'	22		67	0.7	9							0.4	0.6		99.7
115'	15		52	2	4				19			3	1		96.0
120'	14	24	47	2	5				5			2	0.6		99.6
125'	14	29	33	4	16				0.7			2	0.6		99.3
130'	14	24	47	3	4					3	1	0.5	0.8		99.3
135'	17	35	27	4	12					2	0.8		0.9		98.7
140'	20	32	31	5	9					1		0.2	0.7		98.9
145'	23	31	35	4	5					1		0.2	0.6		99.8
150'	12	37	33	5	8					1		0.1	0.6		99
155'	16	37	29	5	10					1		0.4	0.7		99.1
160'	18	28	27	4	21					0.7	0.7	0.4	0.6		100.4
162'	37	28	27	4	3							0.8	0.6		100.4
165'	28	28	31	5	6							0.2		1	99.2
170'	16	36	38	6	2							0.1		2	100.1
175'	17	39	32	7	2							0.1		2	99.1
180'	11	39	33	7	6							0.2		3	99.2
185'	14	40	23	8	12							0.3		3	100.3
190'	13	41	14	8	21							0.3		2	99.3
195'	16	37	24	8	12							0.3		2	99.0
200'	18	38	19	9	13							0.3		3	100.3

MODECALC, unless otherwise stated. Figure 5 shows the major alteration mineralogy as determined by MODECALC.

Alteration Zonation in DDH 1-76

The distribution and abundance of major alteration minerals defines three alteration zones: 1) Advanced Argillic Zone defined by abundant opal and alunite and minor vermiculite and rutile; 2) Argillic Zone defined by abundant kaolinite, occasionally abundant opal (or -α cristobalite) and K-mica, and minor alunite, rutile, and vermiculite; 3) Propylitic Zone defined by abundant K-mica, locally abundant montmorillonite to interlayered illite-montmorillonite, persistant chlorite, occasional calcite, and pyrite. Quartz is stable throughout.

Advanced Argillic Zone (12'-35'). The advanced argillic zone is characterized by quartz, opal, alunite, vermiculite, and rutile. Low a_K/a_H sulfate-waters imposed extreme acid-leaching conditions on the host granitic alluvium. Only quartz (and a small amount of K-spar at 30') were unaffected. K-mica is listed as 5% at 25' in Table 7. Alunite (MODECALC estimation) varies between 24% and 47%. Thin section inspection suggested 30% opal. Abundant opal, common in hot springs deposits, results from quartz saturated solutions at high temperatures (>180^{o}C) at depth becoming oversaturated with respect to quartz and opal as the solution rises and cools (because of very slow quartz precipitation kinetics). The faster precipitation reaction of opal then proceeds at the lower surface temperatures (Krauskopf, 1956; White, et. al., 1971). Some primary quartz grains show elongation and the wavy extinction typical of strained quartz. Vermiculite,

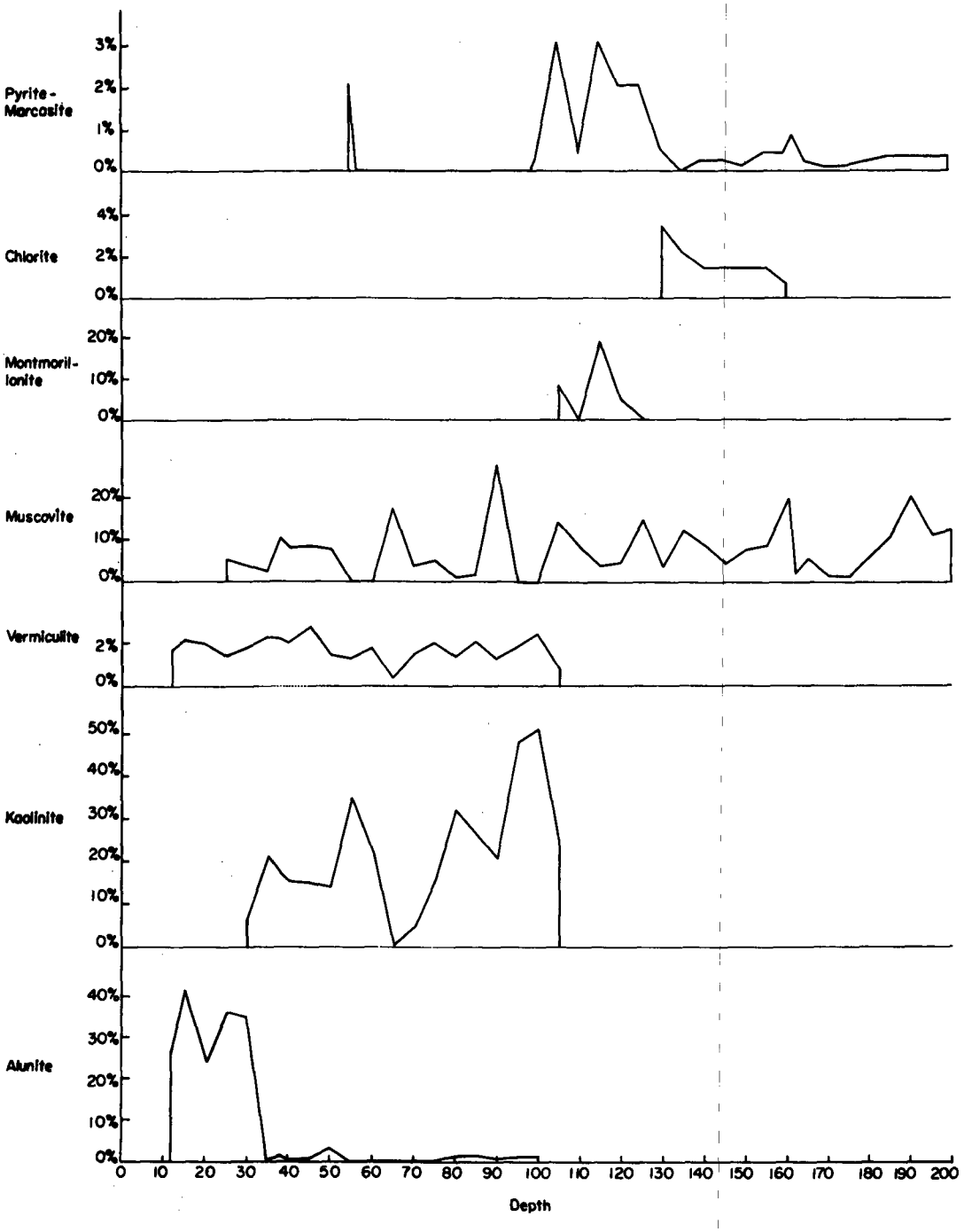

Figure 5. Major Alteration Mineralogy (MODECALC) versus Depth.

which constitutes an average of 2% in this zone, is not described in similar acid-sulfate environments in other geothermal systems. A surprising associate of carbonate (calcite?) with alunite occurs at 12'. The chemical implications of this association will be discussed in the next section.

Argillic Zone (35'-110'). The argillic zone is characterized by abundant kaolinite (15% - 52%), occasionally abundant K-mica, minor alunite, vermiculite and rutile, along with stable quartz, K-spar, and occasionally stable plagioclase. The point count estimates of kaolinite abundance (5% - 12%) are probably low due to the extensive fine-grained groundmass which make reliable optical identification and estimates difficult. Alunite persists in small amounts and K-mica appears.

The 10% K-mica estimate at 38' again was seen in thin section as white mica. A zone (about 5') around 65' is not representative of the rest of the argillic zone. K-spar percentages approach 40%, and even plagioclase (which is almost absent in the rest of this zone) reaches 17%. These feldspars are mostly unaltered. In the 65' thin section, green muscovite replaces biotite and kaolinite is almost absent. At 70', X-ray diffraction gives evidence for vermiculite, which appears abundantly in thin section. Alunite persists through 100', where pyrite is first visibly seen. X-ray diffraction identifies α-cristobalite from 80' through 100'. Carr and Fyfe (1958) suggest that cristobalite occurs midway between amorphous silica and quartz in a crystallization sequence. The abundant groundmass seen in this zone is surely constituted to a large extent by the almost

opaque cristobalite. The argillic zone overlaps with the propylitic zone at 105' where kaolinite (27%) exists for the last time and montmorillonite (8%) first appears.

Propylitic Zone (110'-200'). The propylitic zone has 3 subzones characterized by the following alteration mineral assemblages: 1) montmorillonite + interstratified illite-montmorillonite (montmorillonite dominant) + K-mica + pyrite + rutile; 2) interstratified illite-montmorillonite (illite dominant) + K-mica + pyrite + rutile + > 1% chlorite + > 1% calcite; 3) K-mica + pyrite + small amounts of chlorite and calcite.

The major fracture of this drill hole occurs at 110' where there is mostly unidentifiable groundmass, strained and cryptocrystalline quartz, and some biotite replaced by K-mica and pyrite. At 115', where fault gouge is most prominent, montmorillonite reaches 19% (MODECALC), though the thin sections show mostly unidentifiable groundmass. It should be noted that MODECALC assigns 67-47% orthoclase to the area 110'-130'. This is significantly greater than the K-spar abundance in the fresh quartz monzonite.

Not until 120' does plagioclase (An_{12}) appear in appreciable quantities (24% by MODECALC).

This is consistent with similar observation of Sigvaldason and White (1961) at Steamboat Springs, Nevada. Indeed, plagioclase abundance increases toward 200' as it becomes less the target of alteration.

Chlorite and calcite occur downward from 130', but only in amounts less than 1% after 160'. Their mutual associations have

been previously described. Chlorite replaces both feldspar and biotite with and without calcite, which also occurs in veinlets.

A small fault or fracture at 162' is characterized by fine-grained groundmass, increase in pyrite, and decrease in the content of alkalies. After this zone, rutile (?) finally gives way to sphene from which it has been altering. Sphene occupies 3% (MODECALC) downward to 200'.

Alteration Geochemistry

The alteration zonation seen in DDH 1-76 at the Roosevelt Hot Springs KGRA resulted from the interaction between the hydrothermal fluid and the host rock. The zonation patterns can be considered as: a) a function only of temperature and pH, with fluid composition constant (high flow model) or b) a function of temperature, pH, and fluid composition changing in response to rock alteration reactions (low flow model).

Theoretical activity diagrams, Fig. 6, for temperatures 25°C to 150°C were constructed plotting pH versus log $a_{H_4SiO_4}$ for the phases muscovite, microcline, magnesium montmorillonite, kaolinite, alunite, and gibbsite. Stability field boundaries involving all phases except alunite were calculated using equilibrium constants of Helgeson (1969), and activities for K^+, Mg^{2+}, and $SO_4^=$ as listed in Table 8. Unit activity of water was assumed and aluminum was conserved. Activities for K^+ and SO_4^{2-} at 100°C, 200° and 300°C were these used by Dedolph and Parry (1976). These data were taken from water analyses from Roosevelt Hot Springs (Table 1). An intermediate Mg water analysis value of a_{Mg2+}=.001 was chosen for all temperatures.

Table 8

Log Activity for K^+, Mg^{2+}, SO_4^{2-}, and pH for T=25°C-300°C

Species	25°	60°	100°	150°	200°	250°	300°
K^+	-2.09	-2.10	-2.10	-2.13	-2.15	-2.20	-2.25
Mg^{2+}	-3.38	-3.40	-3.44	-3.52	-3.58	-3.74	-3.90
$SO_4^=$	-3.00	-3.07	-3.10	-3.35	-3.59	-4.30	-4.96
pH	4.5	4.1	3.6	3.3	3.1	3.0	

* These activities are based on the known composition of waters at Roosevelt Hot Springs (Table 1). Data, for K^+ and $SO_4^=$, at temperatures other than 100°C, 200°C, and 300°C were extrapolated from and consistent with those used by Dedolph and Parry (1976). At all temperatures $a_{Mg^{2+}} = .001$, an intermediate value from these water analyses.

At other temperatures, log molalities were interpolated from that data and activity coefficients were calculated from the modified Debye-Hückel equation (Helgeson, 1969).

$$\log \gamma_i = \frac{-A\, Zi^2 \sqrt{I}}{1+\mathring{B}a \sqrt{I}} + \mathring{B}I$$

where γi is the activity coefficient of the i^{th} species with charge Zi: I is the ionic strength, taken to be .1 as used in the study of Dedolph and Parry; A, B, $\mathring{B}$ are solution parameters which are temperature dependent and taken from Helgeson (1969); $\mathring{a}$ is the distance of the nearest approach of ions in solution, taken from Kharaka, et al. (1973).

The stability field of alunite was established by using thermodynamic data from Hemley et al. (1969) and with average heat capacities for the congruent dissolution species of alunite from Criss and Cobble (1964).

Quartz and opal saturation values were taken from solubility curves by Holland (1969). Calcite stability limits were calculated using $m_{Ca}2+ = .002$ as an approximate average of water analyses (Table 1). Maximum pressure estimates were made as follows. At 25^{o}, a surface environment at 1 atm was assumed. At 60^{o}C and 100^{o}C hydrostatic pressure at 60' and 130' (locations in the core where these temperatures exist) was assumed. Values obtained were 1.77 atm and 3.83 atm., respectively. Minimum P_{CO_2} values were estimated as 10^{-3} of the hydrostatic pressure at 12', 60', and 130'. Resultant P_{CO_2} minimum values were .0003, .0018, and .0038 atm. Activity co-

efficients $\gamma_{Ca^{++}}$, $\gamma_{HCO_3^-}$, and $\gamma_{CO_3^{--}}$ were calculated from the modified Debye-Hückel equation. $\gamma_{H_2CO_3}$ was assumed to equal 1 and the ionic strength was assumed to equal 0.1.

The second set of activity diagrams (Figure 7) for T=25° - 100°C plots log a^2_{H+} $a_{SO_4^=}$ vs. log a^2_{K+} $a_{SO_4^=}$ (after Hemley et. al., 1969) and also for T=100°C, plots log a^2_{H+} $a_{SO_4^=}$ vs log a_{K^+}/a_{H^+} (after Dedolph and Parry, 1976). All diagrams illustrate the phase relationships for both opal and quartz saturation. Hydrolysis equilibrium constants for all phases in diagrams a, b, and c were taken from Helgeson (1969), except for alunite, taken from Kharaka, et. al (1973). All hydrolysis constants in Figure 7d were taken from Kharaka, et. al. except for muscovite, taken from Helgeson.

A third set of activity diagrams, Figure 8, plots log a_{k^+}/a_{H^+} vs log $a_{Mg^{2+}}/a^2_{H^+}$ at temperatures 25°C-150°C. Both quartz and opal saturation diagrams are shown for the phases kaolinite, muscovite (occurring only at 150°C, quartz saturation), microcline, Mg-montmorillonite, and chlorite (clinochlore). All hydrolysis equilibrium constants were taken from Helgeson (1969) and unit activity of water was assumed. Aluminum was always conserved.

The activity diagrams in Figures 6, 7, and 8 are meant to represent the major alteration phases observed at Roosevelt Hot Springs. There are some obvious omissions which warrant discussion. Even though plagioclase (An_{12}) is a major reactant mineral, there are appreciably no sodium product minerals (except for minor sodium in montmorillonite); therefore no a_{Na} diagrams. Biotite is a second mineral having shown consistent alteration to vermiculite and iron-

Figure 6. pH vs log $a_{H_4SiO_4}$ activity diagrams for the phases alunite, gibbsite, kaolinite, Mg-montmorillonite, muscovite, and microcline, at temperatures 25°C, 60°C, 100°C, and 150°C. The maximum calcite stability limits (lowest pH limit) for 25°C, 60°C, and 100°C are: P_{CO_2} = 1 atm, P_{CO_2} = 1.8 atm, and P_{CO_2} = 3.8 atm. The minimum calcite stability limits for these temperatures are: P_{CO_2} = .0004 atm, P_{CO_2} = .002 atm, and P_{CO_2} = .004 atm. For all diagrams $M_{Ca^{2+}}$ = .002, $m_{Mg^{2+}}$ = .001, and a_{H_2O} = 1. Activities for K^+, SO_4^{2-}, and Mg^{2+} are listed in Table 8 . The following legend applies:

_ _ _ _ maximum calcite stabiltiy

_ - _ - _ minimum calcite stability

_____ quartz saturation

---------- opal saturation

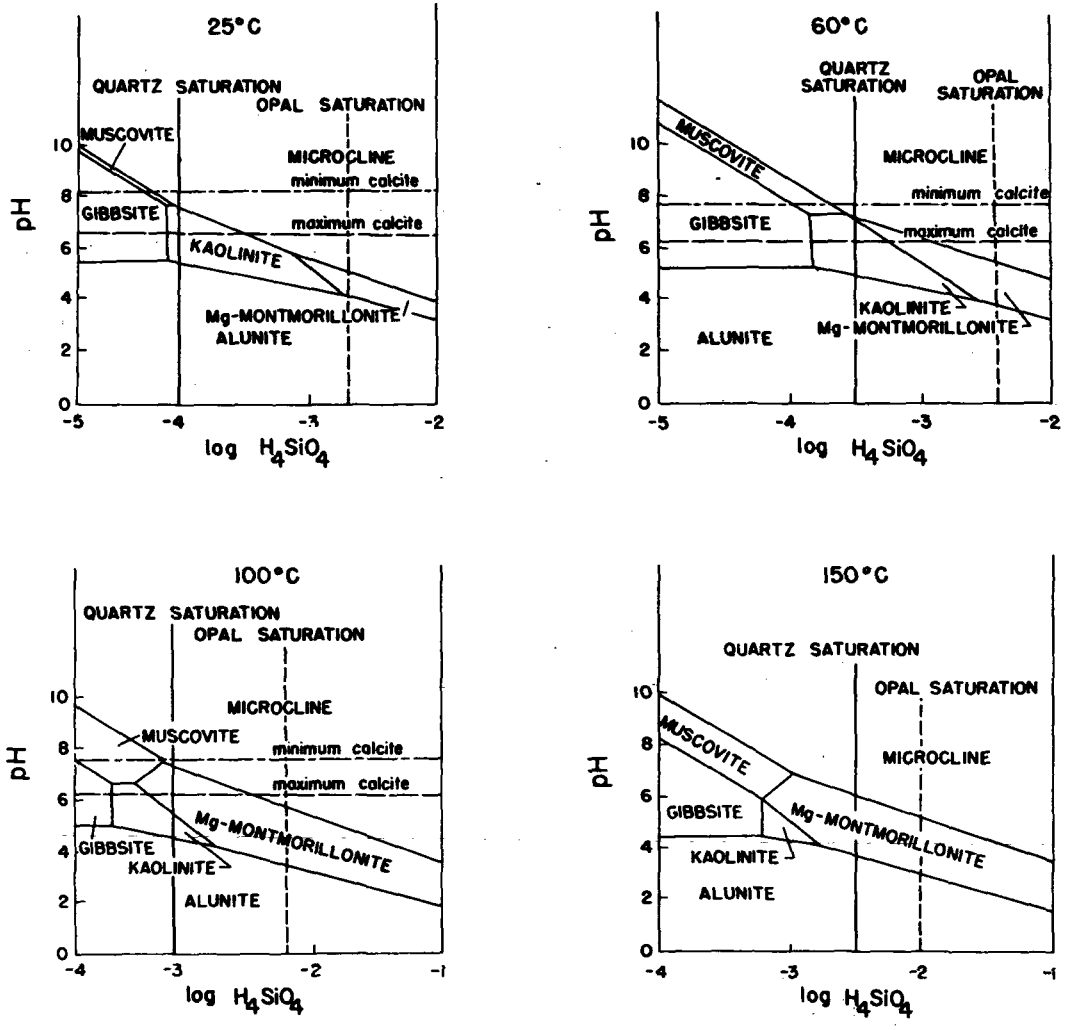
25°C
QUARTZ SATURATION
OPAL SATURATION
MUSCOVITE
MICROCLINE
minimum calcite
GIBBSITE
maximum calcite
KAOLINITE
Mg-MONTMORILLONITE
ALUNITE
pH
log H4SiO4
60°C
QUARTZ SATURATION
OPAL SATURATION
MUSCOVITE
MICROCLINE
minimum calcite
GIBBSITE
maximum calcite
KAOLINITE
Mg-MONTMORILLONITE
ALUNITE
pH
log H4SiO4
100°C
QUARTZ SATURATION
OPAL SATURATION
MICROCLINE
MUSCOVITE
minimum calcite
maximum calcite
Mg-MONTMORILLONITE
GIBBSITE
KAOLINITE
ALUNITE
pH
log H4SiO4
150°C
QUARTZ SATURATION
OPAL SATURATION
MUSCOVITE
MICROCLINE
GIBBSITE
Mg-MONTMORILLONITE
KAOLINITE
ALUNITE
pH
log H4SiO4

Figure 7. Activity diagrams plotting log $a^2_{H+}\ a_{SO_4=}$ vs log $a^2_{K+}\ a_{SO_4=}$ for T = 25°C, 60°C, and 100°C for the phases kaolinite, alunite, and K-mica. Both quartz and opal saturation are shown.

At 100°, an activity diagram plotting log $a^2_{H+}\ a_{SO_4=}$ vs log a_{K+}/a_{H+} represents the phases alunite, kaolinite, muscovite, and microcline. Quartz saturation is assumed.

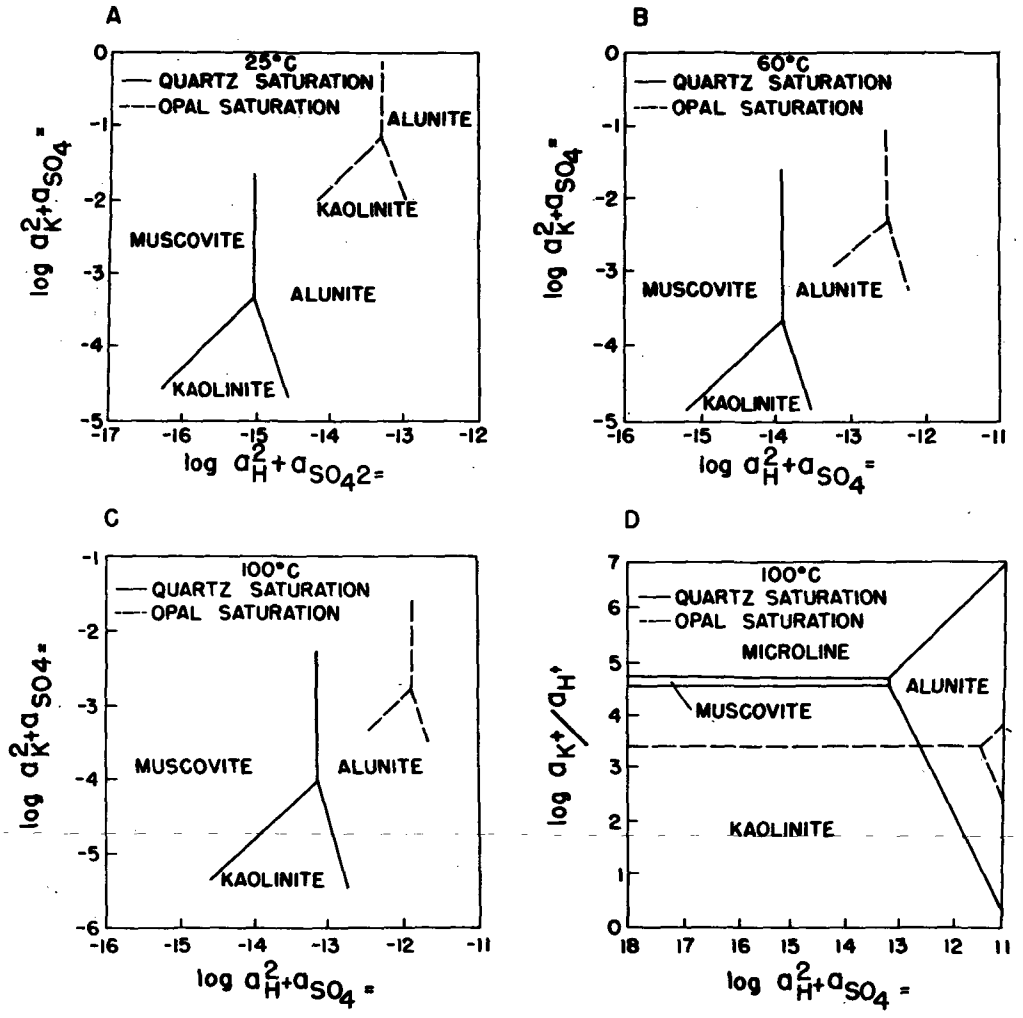
A
25°C
QUARTZ SATURATION
OPAL SATURATION
ALUNITE
KAOLINITE
MUSCOVITE
ALUNITE
KAOLINITE
log $a_K^2+a_{SO_4}$=
log $a_H^2+a_{SO_4}$2=
B
60°C
QUARTZ SATURATION
OPAL SATURATION
MUSCOVITE
ALUNITE
KAOLINITE
log $a_K^2+a_{SO_4}$=
log $a_H^2+a_{SO_4}$=
C
100°C
QUARTZ SATURATION
OPAL SATURATION
MUSCOVITE
ALUNITE
KAOLINITE
log $a_K^2+a_{SO4}$=
log $a_H^2+a_{SO_4}$=
D
100°C
QUARTZ SATURATION
OPAL SATURATION
MICROLINE
ALUNITE
MUSCOVITE
KAOLINITE
log a_{K^+}/a_{H^+}
log $a_H^2+a_{SO_4}$=

Figure 8. Activity diagrams plotting log a_{K+}/a_{H+} vs log $a_{Mg^{2+}}/a^2_{H+}$ for T = 25^{o}-150^{o}C for the phases kaolinite, muscovite, microcline, Mg-montmorillonite, and chlorite (clinochlore). Aluminum was conserved in all reactions. Diagrams for both quartz and opal saturation are shown.

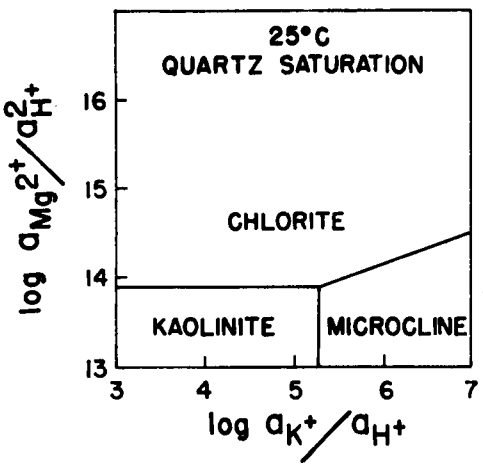
25°C
QUARTZ SATURATION
CHLORITE
KAOLINITE
MICROCLINE
log $a_{Mg^{2+}}/a_{H^+}^2$
log a_{K^+}/a_{H^+}

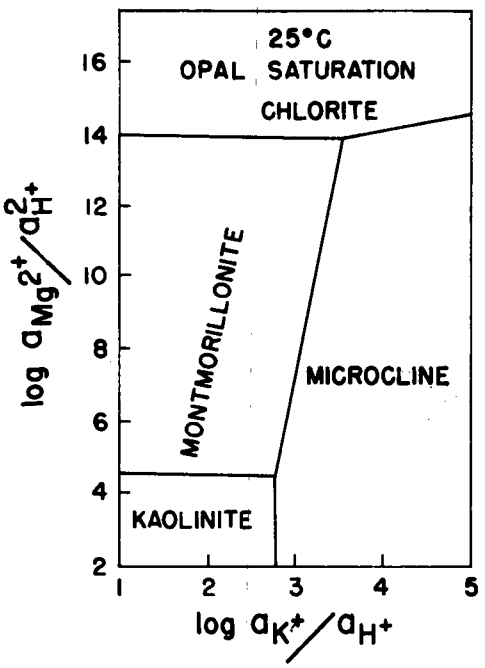
25°C
OPAL SATURATION
CHLORITE
MONTMORILLONITE
MICROCLINE
KAOLINITE
log $a_{Mg^{2+}}/a_{H^+}^2$
log a_{K^+}/a_{H^+}

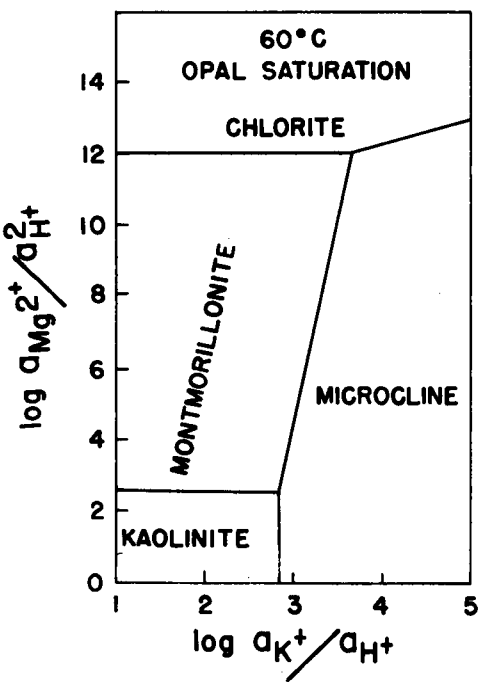
60°C
OPAL SATURATION
CHLORITE
MONTMORILLONITE
MICROCLINE
KAOLINITE
log $a_{Mg^{2+}}/a_{H^+}^2$
log a_{K^+}/a_{H^+}

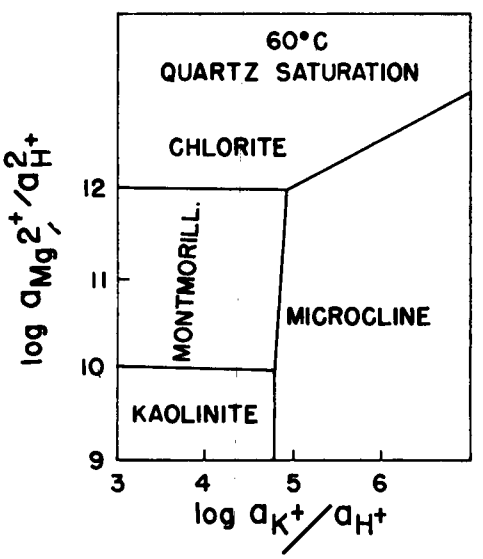
60°C
QUARTZ SATURATION
CHLORITE
MONTMORILL.
MICROCLINE
KAOLINITE
log $a_{Mg^{2+}}/a_{H^+}^2$
log a_{K^+}/a_{H^+}

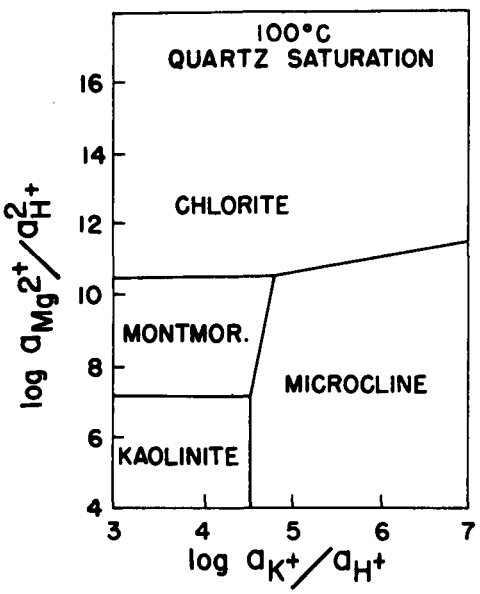
100°C
QUARTZ SATURATION
CHLORITE
MONTMOR.
MICROCLINE
KAOLINITE
log $a_{Mg^{2+}}/a_{H^+}^2$
log a_{K^+}/a_{H^+}

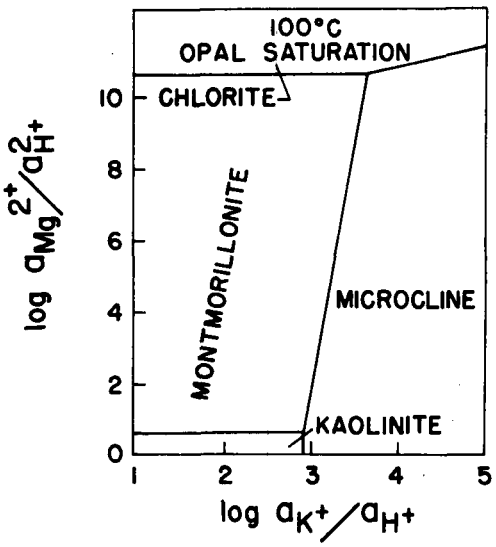
100°C
OPAL SATURATION
CHLORITE
MONTMORILLONITE
MICROCLINE
KAOLINITE
log $a_{Mg^{2+}}/a_{H^+}^2$
log a_{K^+}/a_{H^+}

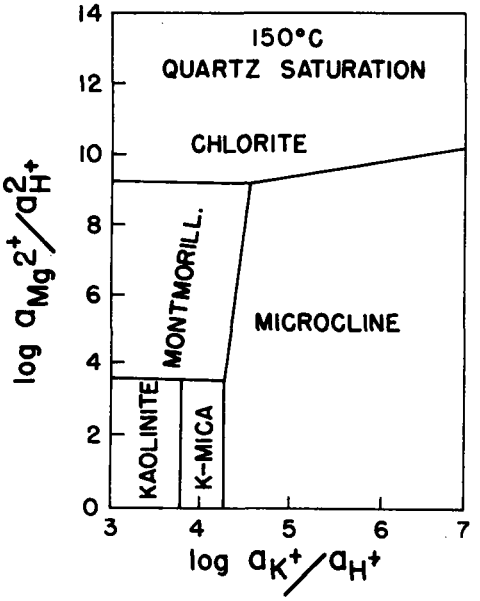
150°C
QUARTZ SATURATION
CHLORITE
MONTMORILL.
MICROCLINE
KAOLINITE
K-MICA
log $a_{Mg^{2+}}/a_{H^+}^2$
log a_{K^+}/a_{H^+}

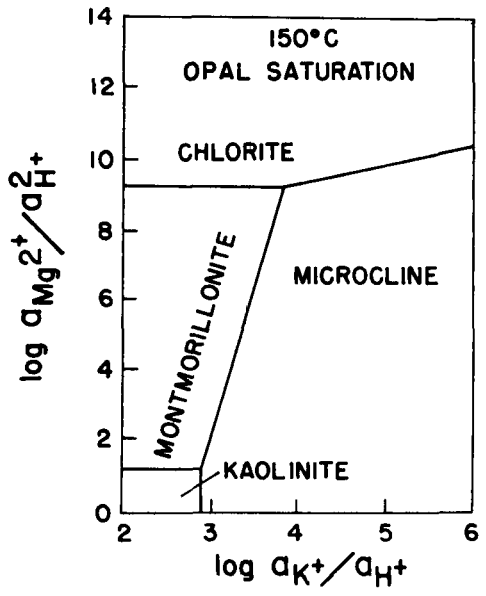
150°C
OPAL SATURATION
CHLORITE
MONTMORILLONITE
MICROCLINE
KAOLINITE
log $a_{Mg^{2+}}/a_{H^+}^2$
log a_{K^+}/a_{H^+}

rich muscovite. Even though thermodynamic data for vermiculite were calculated (Appendix 3), the absence of reliable a_{Fe}^{3+} and a_{Fe}^{2+} data made sensible activity diagrams including vermiculite impossible

These activity diagrams have been presented in order to clarify chemical relationships between alteration minerals and to suggest pathways which the hydrothermal fluids may have travelled.

Dedolph and Parry (1976) modeled the hydrolysis of microcline in acid sulfate waters consistent with water composition at Roosevelt Hot Springs. Their model of a 100°C solution, with an initial pH= 3.6 is shown here as Figure 9. The variable ξ is a function of time. At the top of the figure are the major events which occur while the solution is moving toward equilibrium with microcline. Minerals are precipitated in the order: quartz, alunite, kaolinite, and muscovite. This system is consistent with the alteration in DDH 1-76 above 120'. Calculations for Figure 9 do not consider montmorillonite, calcite, and chlorite, which occur below 120', because of the tacit assumption that the activities of Mg^{2+} were too low for the intersection of these fields.

Figure 7 considers the same stability relations as the reaction path diagram. The coordinates for initial solution composition (from Table 8) for each of the diagrams are listed in Table 9. The initial solution coordinates for Figure 7a and Figure 7b fall in the alunite field for quartz saturation and in the kaolinite field at opal saturation. In both cases (opal and quartz saturation) of the 100° diagrams, the initial solution intersects the alunite field. A downward moving, low-pH, boiling water that is opal saturated could

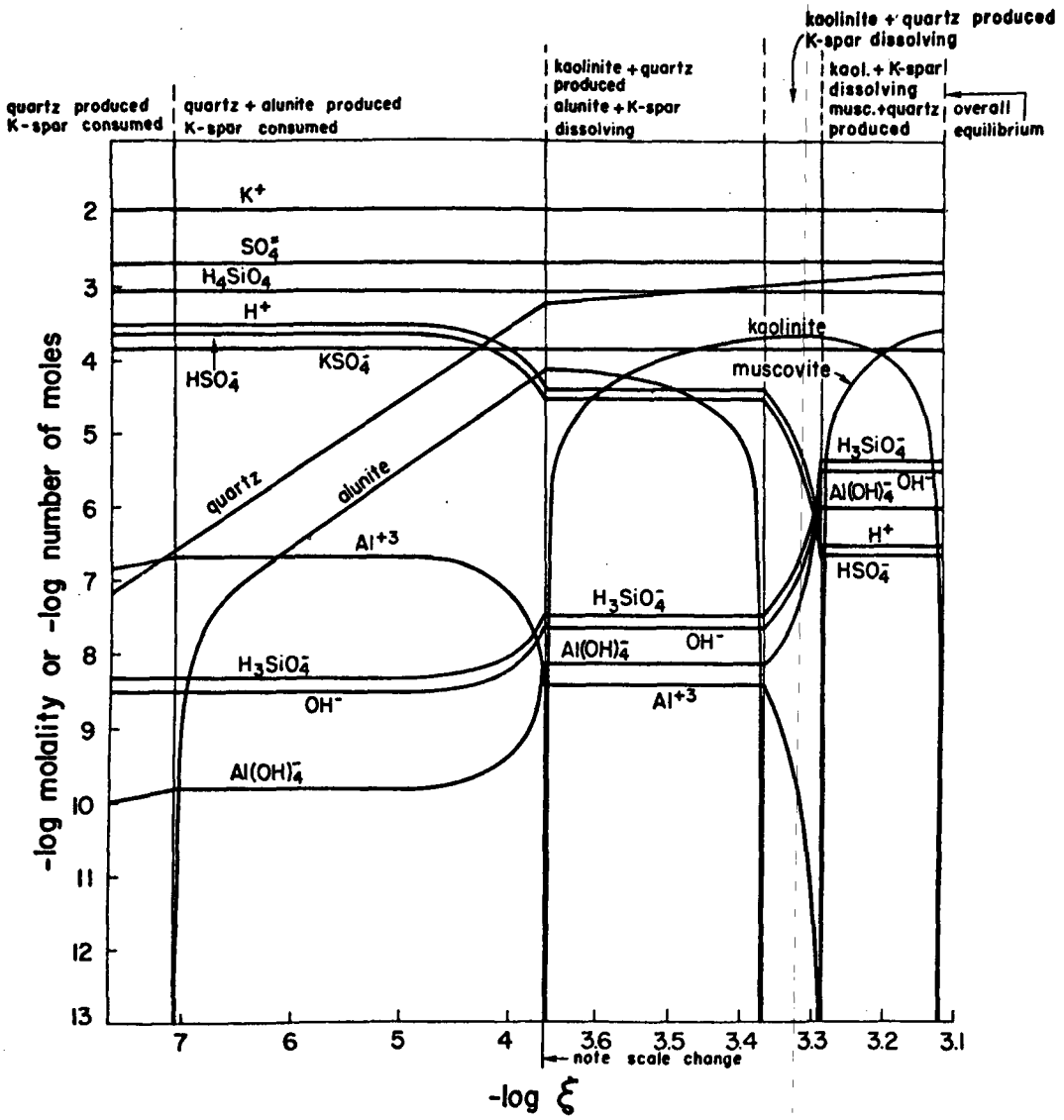

Figure 9. Reaction path for the dissolution of microcline at 100°C and initial solution pH = 3.6 (Dedolph and Parry, 1976).

Table 9. Initial Solution Compositions for Figures 7 and 8

Figure	Solution Coordinates			
	$\log a_H^2 a_{SO_4}$	$\log a_K^2 a_{SO_4}$	$\log a_K/a_H$	$\log a_{Mg}/a_H^2$
6a, 25°	-12	-7.18		
6b, 60°	-11.27	-7.27		
6c, 100°	-10.30	-7.30		
6d, 100°	-10.30		1.5	
7 , 25°			2.41	5.62
7 , 60°			2.00	4.80
7 , 100°			1.50	3.76
7 , 150°			1.20	3.08

produce the sequence opal + alunite, opal + alunite + kaolinite, opal + kaolinite + muscovite. Upper waters, below boiling, could produce the same assemblages, except for the subsitution of quartz for opal. Opal saturation requires higher a_{H+}, a_{K+}, and $a_{SO_4^{2-}}$ to reach the alunite - kaolinite - muscovite triple point.

Figures 6 and 8 differ from the previous figures by including the magnesium phases montmorillonite and chlorite (and calcite in Figure 6), which occur below 120' in DDH 1-76. These diagrams include pure magnesium end members.

Figure 6 suggests several observations: 1) If a solution has an $a_{Mg^{2+}}$ high enough to warrant a sizeable Mg-montmorillonite field, and if that solution is restricted to a_{SiO_2} between quartz and opal saturation, then increasing pH solutions can produce opal with alunite and Mg-montmorillonite; or they can produce quartz with alunite, Mg-montmorillonite and kaolinite at and below 100°C. 2) If $a_{Mg^{2+}}$ is decreased and a_{K+} is increased, the muscovite field can be intersected at quartz saturation at and below 100°C, and at opal saturation only at 100°C. 3) At the assumed ion activities, muscovite can be formed only in a solution under saturated with respect to quartz. 4) Calcite is incompatible with alunite at all temperatures and is compatible with Mg-montmorillonite (as seen below 120') above 60°C if $P_{CO_2} \leq$ hydrostatic pressure. Alunite occurs with calcite at 12' in DDH 1-76. Ransome (1909) noted one occurrence of calcite with alunite, kaolinite, and sericite at Goldfield, Nevada. He suggested that CO_2 was trapped and resulted in abnormally high P_{CO_2}.

Figure 8 invites the following observations: 1) Only at 150°C

and quartz saturation is the a_{K+} assumption sufficiently high to produce a muscovite stability field. 2) At quartz saturation initial solution compositions (Table 9) intersect the kaolinite field; while at opal saturation these initial solutions intersect the Mg-montmorillonite field. 3) A solution saturated with quartz and an upward path with a positive slope, can produce (except for muscovite) the observed alteration sequence of kaolinite, montmorillonite, and chlorite.

These observations suggest some explanations for the observed mineralogy, and also offer some problems for that explanation. In considering Figures 6, 7, and 8 together, an increasing pH model at quartz saturation can account for the sequence alunite, kaolinite, muscovite, montmorillonite, calcite, and chlorite, as depth and temperature increase. The major problems are: 1) the difficulty of intersecting the muscovite field and 2) the difficulty of producing opal with kaolinite and muscovite. Several possible schemes to reconcile these problems follow. These models overlap and, instead of each one providing a complete explanation, each model proposes a different mechanism to explain certain aspects of the observed alteration.

Model 1. Model 1 assumes an a_{K+} large enough for the muscovite field to intersect the quartz saturation boundary. At depth, with temperatures in excess of 200°C, the solution is slightly basic and saturated with respect to quartz. As this fluid rises along a fracture (possibly the fault at 115' in the core) and the temperature drops below 180°, the solution becomes super-saturated with quartz.

As pH slowly increases, or perhaps remains constant, the solutions produce chlorite, montmorillonite (lowering $a_{Mg}2+$), calcite, muscovite (and illite). As the fluids pass the water table at 115', the tendency for pH to increase is overcome by the acid-producing reaction oxidizing sulfide to sulfate. As pH decreases and silica activities trend toward opal saturation, the kaolinite and finally opal fields are intersected. These low pH, low $a_{Mg}2+$, and opal-saturated solutions then percolate downward (similar to the mechanism proposed for Steamboat Springs, Nevada, by Schoen, White, and Hemley, 1974) on a path of increasing pH and decreasing a_{SiO_2}. On the downward path the alunite, kaolinite and muscovite fields are intersected. The downward solutions reach equilibrium with microcline rather than intersecting the montmorillonite and chlorite fields.

Model 2. Model 2 is a vapor dominated system (idea modified from the discussion of vapor-dominated hydrothermal systems by White, Muffler, and Truesdell, 1971), in which condensed vapors are under-saturated with respect to quartz. A solution which condenses at, perhaps 150^{o} (at approximately 130'), could intersect the muscovite field and intersect the montmorillonite, kaolinite and alunite fields as the solution rises. It is doubtful that such a solution would ever reach opal saturation, however.

Model 3. This model proposes two non-contemporaneous solutions, each producing a desired assemblage. Solution A is a high $a_{Mg}2+$ fluid (saturated with quartz) which, by the time it reaches 200', intersects the chlorite stability field, then the montmorillonite field. At

about 100', opal saturation within the montmorillonite stability field is reached. This alteration assemblage is maintained to the surface. Solution B is a low a_{Mg}^{2+} fluid (too low for the existence of magnesium minerals) which is saturated or super-saturated with respect to quartz. As solution B rises above the water table, the oxidation of sulfate lowers the pH. At the surface, the fluid is in the alunite field, destroying the previously formed montmorillonite. With downward percolation, alteration proceeds to kaolinite and muscovite. At 120', muscovite continues to replace montmorillonite (as well as biotite and feldspar), but not completely.

These three models, which contain abundant fiction, illustrate the complexity of identifying the geochemical alteration process. Additional studies could help clarify the situation. The identification of secondary K-feldspar, and its relationship to other minerals would help restrict pH and a_{K^+} values. Microprobe work to determine the compositions of primary biotite and secondary vermiculite, along with Fe^{3+} and Fe^{2+} determinations in the water, would further clarify Eh-pH and Mg^{2+} conditions.

HEAT FLOW CONTRIBUTIONS FROM HYDROTHERMAL ALTERATION

Most hydrothermal alteration reactions for minerals in DDH 1-76 are exothermic (Table 10). These exothermic reactions may generate a significant amount of heat compared to the heat flow of the area and compared to the heat generated by a cooling granitic magma.

The problems of making a sensible determination lie in: 1) the extent, laterally and vertically, of the alteration and 2) the time over which the hot springs have been active. The time problem has already been discussed. Reasonable maximum and minimum time limits from that discussion are 0.4 m.y. and 0.01 m.y., respectively. If the activity has been episodic, these times are further reduced. For purposes of calculations here, activity of the geothermal area for 10% of the above times will be assumed, resulting in .04 m.y. and .001 m.y.

Some estimation of the lateral and vertical extent of alteration has been gained through Schlumberger and electro-magnetic depth soundings (Tripp, 1977) and by dipole-dipole resistivity surveys (Ward and Sill, 1976).

The two geologic interpretation diagrams of Tripp (Figures 18 and 19 of that publication) broadly suggest a fractured and highly altered zone, bounded to the east and west by saturated altered rock and alluvium, and underlain by resistive (unaltered) bedrock. The saturated altered rock and alluvium varies in thickness from

Table 10. Reactions Used in Reaction Enthalpy Calculations

Reaction No.	Reaction
1	$3KAlSi_3O_8 + 2SO_4^{2-} + 6H^+ = KAl_3(SO_4)_2(OH)_6 + 2K^+ + 9SiO_2(\alpha\text{-qtz})$
2	$3NaAlSi_3O_8 + 2SO_4^{2-} + 6H^+ + K^+ = KAl_3(SO_4)_2(OH)_6 + 3Na^+ + 9SiO_2(\alpha\text{-qtz})$
3	$H_4SiO_4 = 2H_2O + SiO_2(\alpha\text{-qtz})$
4	$CaTiOSiO_4 + 2H^+ = Ca^{2+} + TiO_2(\text{rutile}) + SiO_2(\alpha\text{-qtz})$
5	$3KAlSi_3O_8 + 2H^+ = KAl_3Si_3O_{10}(OH)_2 + 6SiO_2(\alpha\text{-qtz}) + 2K^+$
6	$2KAlSi_3O_8 + 2H^+ + 2H_2O = Al_2Si_2O_5(OH)_4 + 2K^+ + 4SiO_2(\alpha\text{-qtz})$
7	$2NaAlSi_3O_8 + 2H^+ + 2H_2O = Al_2Si_2O_5(OH)_4 + 2K^+ + 4SiO_2(\alpha\text{-qtz})$
8	$H_2S + 2O_2(g) = 2H^+ + SO_4^{2-}$
9	$Fe^{2+} + S^{2-} + 1/2\,S_2 = FeS_2(\text{pyrite})$
10	$KMg_{1.8}Fe^{2+}_{1.2}Si_3AlO_{10}(OH)_2 + 3.2Mg^{2+} + .3O_2 + 4SiO_2 + 11.4H_2O = K^+ + 4.8H^+ + 2Mg_{.25}Mg_{2.25}Fe^{3+}_{.5}Al_{.5}Si_{3.5}O_{10}(OH)_2 \cdot\cdot 4H_2O + .2Fe^{3+}$
11	$2KMg_3AlSi_3O_{10}(OH)_2 + 4H^+ = 2K^+ + 3SiO_2 + Mg_5Al_2Si_3O_{10}(OH)_8 + Mg^{2+}$
12	$14NaAlSi_3O_8 + 12H^+ + Mg^{2+} = 6Mg_{.167}Al_{2.33}Si_{3.67}O_{10}(OH)_2 + 14Na^+ + 20SiO_2$
13	$CO_3^{2-} + Ca^{2+} = CaCO_3$

approximately 75 - 400 meters, with greatest thickness lying to the west. The deep conductive layer to the west, however, may be due not so much to alteration, as from warm brines leaking from the system (Ward and Sill, 1976). Additional information from Ward and Sill at 8100N indicates a resistive contact at 500m, probably, though not certainly, due to decreased alteration.

Given the pH and K^+ values for the deep reservoir, Table 1, analysis 4, K-feldspar can be expected to be stable at 150°C. With thermal gradients ranging from 460°C/km (DDH 1B) to 937°C/km (DDH 1-76), the K-spar stable zone occurs at depths of 326 - 160 meters.

Method

For each secondary phase in DDH 1-76, a chemical reaction was written (Table 10). For each chemical species in the thirteen reactions, standard enthalpies of formation (ΔH_f) and heat capacities (Cp) are listed in Table 11. Only ΔH_f and Cp for biotite-.6 phlogopite and vermiculite were calculated (Appendix 3); all other data were readily available in cited references. All the average heat capacity data for ions and H_4SiO_4 were taken from Helgeson (1969). A straight line equation was calculated based on the average heat capacities at 60°C and 100°C. This process introduces little error since an average heat capacity represents nothing more than the first term in the heat capacity power function. Over small temperatures ranges, the second and third power function terms are small and linearity is closely approached.

This equation was assumed to be valid everywhere in the temperature

Table 11. Thermodynamic Data for Reaction Enthalpy Calculations

Species	C_p[a] a	C_p[a] $bx10^3$	C_p[a] $cx10^{-5}$	$\overline{Cp}$[b]	ΔH_f(25°C)-cal/gfw	Data Source ΔH	Cp	$\overline{Cp}$
$KAlSi_3O_8$ - microcline	63.83	12.90	-17.05		-946,000	1	1	
$NaAlSi_3O_8$ - low albite	61.70	13.90	-15.01		-937,300	1	1	
$KAl_3(SO_4)_2(OH)_6$	231	78.60	-67.80		-1,235,600	4	5	
SiO_2-α-quartz	11.22	8.20	-2.70		-217,650	2	2	
H_4SiO_4				49	-348,060	1		1
$CaTiOSiO_4$	42.39	5.54	-9.63		-622,050	3	3	
TiO_2 - rutile	17.97	0.28	-4.35		-225,760	3	3	
H_2O-(l)	18.04				-68,315	2	2	
$KAl_3Si_3O_{10}(OH)_2$	97.56	26.38	-25.44		-1,420,900	1	1	
$KMg_3AlSi_3O_{10}(OH)_2$ (phlogopite)	96.36	26.53	-27.23		-1,499,760	6	6	
$KMg_{1.8}Fe_{1.2}Si_3AlO_{10}(OH)_2$ (biotite-.6 phlogopite)	98.18	31.07	-18.58		-1,391,576	6	6	
$Mg_5Al_2Si_3O_{10}(OH)_8$ (Mg-chlorite)	148.5	36.1	-23.90		-2,109,840	1	1	
$Mg_{.167}Al_{2.33}Si_{3.67}O_{10}(OH)_2$ (Mg-montmorillonite)	84.0	33.7	-19.90		-1,364,140	1	1	
$Mg_{2.8}Fe^{+3}_{.5}Si_{2.9}Al_{1.1}O_{10}(OH)_2 \cdot 4H_2O$ (vermiculite)	118.89	33.46	-16.29		-1,630,439	7	7	
$CaAl_2Si_2O_8$	64.42	13.70	-16.89		-1,009,300	1	3	
$CaCO_3$ - Calcite	24.98	5.24	-6.20		-288,420	1	1	
FeS_2 - Pyrite	17.88	1.32	-3.05		-41,000	2	1	

Table 11 (Continued)

Species	Cp a	Cp $bx10^{-3}$	Cp $cx10^{5}$	$\overline{Cp}$	ΔH_f(25°C)-cal/gfw	Data Source ΔH	Cp	$\overline{Cp}$
$Al_2Si_2O_5(OH)_4$	67.93	19.22	-13.78		-980,020	1	1	
H^+				$.2T^{\circ K}$ - 43.6	0	1		1
K^+				$.2T^{\circ K}$ - 39.60	-60,040			
Na^+				$.15T^{\circ K}$ - 14.95	-57,279	1		1
Ca^{2+}				$.35T^{\circ K}$ - 71.55	-129,770	1		1
Mg^{2+}				$.40T^{\circ K}$ - 109.20	-110,410	1		1
Fe^{2+}				$.41T^{\circ K}$ - 86.35	-21,000	1		1
Fe^{3+}				$.91T^{\circ K}$ - 232.98	-11,400	1		1
Al^{3+}				$.58T^{\circ K}$ - 120.84	-127,000	1		1
CO_3^{2-}				$-.35T^{\circ K}$ - 15.45	-161,840	1		1
SO_4^{2-}				$-.23T^{\circ K}$ - 22.70	-217,320	1		1
S^{2-}				$-.25T^{\circ K}$ + 35.35	9,070	1		1
$H_2S(g)$	7.81	2.96	-0.46		-4,930	1	1	
$CO_2(g)$	10.57	2.10	-2.06		-94,050	1	1	
$O_2(g)$	7.16	1.00	-0.40		0	1	1	
$S_2(g)$	8.72	0.16	-0.90		30,680	1	1	

[a] Heat Capacity Power Function Coefficients. Cal/gfw-°K.

[b] Average heat capacities (Helgeson, 1969) for 60°C and 100°C were used to define a line to compute an average heat capacity for each temperature zone. Cal/gfw-°K.

[1] Helgeson (1969) [2] Robie and Waldbaum (1968) [3] Kelley (1960) [4] Hemley et al. (1969)

[5] Miller (1976) [6] Beane (1972) [7] calculated, this report.

range 33°C to 105°C. It is this straight line equation that is listed in Table 11. The enthalpy of reaction at an elevated temperature, $\Delta H_r(T)$, is calculated by equation 1.

$$\Delta H_r(T) = \Delta H_r^o\ (25^oC) + \int_{25^o}^{T} \Delta Cp\ dT \qquad (1)$$

where

$$\Delta Hr\ (25^o) = \sum_{i=1}^{n} \Delta H_f(25^o) - \sum_{j=1}^{m} \Delta H_f(25^o) \qquad (2)$$

and

$$\Delta Cp = \sum_{i=1}^{n} Cp_{products} - \sum_{j=1}^{m} Cp_{reactants} \qquad (3)$$

The integral of the average heat capacity is simply

$$\int_{T_o}^{T} \overline{Cp}\ \ dt = \overline{Cp}\ (T-T_o). \qquad (4)$$

The integral of a heat capacity power function is

$$\int_{T_o}^{T} CpdT = a(T-T_o) + \frac{b}{2}\ (T^2-T_o^2)x10^{-3} - c(\frac{1}{T} - \frac{1}{T_o})x10^5 \qquad (5)$$

where a, b, c are heat capacity power function coefficients.

The drill hole was divided into seven approximately 11°C interval temperature zones. Actual temperature measurements of DDH 1-76 (Sill, 1977, Appendix 4) were plotted versus depth and a temperature thereby chosen for each sample depth. The average of these temperatures was calculated for each zone. For each reaction in Table 10 the enthalpies of reaction for each appropriate temperature zone are listed in Table 12.

At each depth, the number of moles of each product mineral per 100 gm (including excess silica) was calculated along with the heat of reaction to produce that amount of product. The sum of the

Table 12. Reaction Enthalpies for 7 Temperature Zones* of DDH 1-76

	Reaction Enthalpy - Calories						
Reaction No.[a]	33°C	48.6°C	61.7°C	72.8°C	84.4°C	96.3°C	105.1°C
1	-39,625	-35,436	-32,760	-30,077	-27,360		
2	-57,226	-52,671	-49,743	-46,886	-44,019		
3	-6,237	-6,266	-6,286	-6,300	-6,312	-6,325	-6,335
4	-19,374	-19,256	-19,178	-19,127	-19,088	-19,064	
5	-8,744	-8,735	-8,704	-8,680	-8,657	-8,633	-8,615
6	-10,437	-10,546	-10,644	-10,730	-10,822	-10,919	
7		-21,936	-21,811	-21,735	-21,685		
8	-213,024	-214,212	-215,148	-215,892	-216,623		
9			-43,901	-43,658	-43,360	-43,008	-42,717
10	-29,256	-29,888	-30,393	-30,804	-31,215		
11				5,435	5,233	5,022	4,866
12				-101,933	-101,270	-100,452	-100,149
13				8,336	8,598	10,897	11,861

[a]Reactions are listed by number in Table 10.

*33° (12'-25'), 48.6° (30'-40'), 61.7° (40'-65'), 72.8° (65'-90')
84.4° (90'-125'), 96.3° (125'-162'), and 105.1° (162'-200')

reaction enthalpies, Q/m (cal/g), for each sample were multiplied by estimated densities to obtain the quantity Q/v (cal/cm^3) listed in Table 13. The negative sign denotes the exothermic nature of the reactions. There are three columns for each thermal gradient, which differ in the extent to which the sulfide to sulfate reaction occurred to supply the sulfate ion for the formation of alunite. Water analysis from the deep reservoir (Table 1) indicates that there is abundant $SO_{4=}$ in the deep reservoir. The three values chosen for sulfur oxidation (0%, 10%, 100%) result in a wide range of values in the upper 35' where there is abundant alunite. As alunite becomes much less significant below 35', so does the oxidation of sulfide.

The relationship

$$q = (Q/v) \times \frac{\text{depth}}{\text{time}}$$

enables estimation of heat flow due to hydrothermal alteration. Table 14 lists the assumptions and resultant heat flow which range from 0.02 to 67 HFY. The average thermal gradient is $937^{o}C/km$ for a thermal conductivity of $4X10^{-2}$ $\mu cal/cm\text{-}sec\text{-}^{o}C$: the resultant heat flow is 37 HFU. The 200' estimate is merely to show what fraction of the heat flow the known 200' of alteration adds. Extrapolations to other depths were made by assuming uniform alteration (K-mica and pyrite), as seen in the lower 15' of the core with constant reaction enthalpies.

It is not known whether these temperatures are actually those present at the time of the alteration. A logical upper bound on temperature would be to assume boiling water. Boiling water temperature gradients for various salinities are available (Haas, 1971).

Table 13

Total Heats of Reaction per Unit Volume

	Present-Day Thermal Gradient [b]			Boiling-Water Thermal Gradient [c]		
Depth-ft.	cal/cm^3*	cal/cm^3**	cal/cm^3***	cal/cm^3*	cal/cm^3**	cal/cm^3***
12	-74	-126	-597	-50	-96	-500
15	-98	-177	-902	-61	-133	-868
20	-72	-228	-547	-48	-96	-529
25	-92	-158	-797			
30	-88	-158	-800	-59	-132	-787
35	-64	-66	-82			
38	-56	-59	-89			
40	-55	-57	-72	-54	-56	-72
45	-64	-67	-89			
50	-54	-62	-136			
55	-83					
60	-52	-53	-65	-49	-50	-61
65	-20	-21	-29			
70	-24	-25	-34			
75	-54	-55	-66			
80	-73	-76	-104	-68	-71	-100
85	-74	-78	-116			
90	-50	-53	-74			
95	-78	-82	-111			
100	-85			-77		
105	-117					
110	-16					
115	-135					
120	-46			-43		
125	-26					
130	-6.6					
135	-7.0					
140	-8.2					
145	-5.6					
150	-5.8			-4.5		
155	-9.7					
160	-13					
162	-30					
165	-17					
170	-9.0					
175	-7.9					
180	-5.8			-5.7		
185	-9.2					
190	-14					
195	-9.7					
200	-9.8					

* does not include oxidation of any sulfide to sulfate
**includes oxidation of sulfide to 10% sulfate
*** includes oxidation of sulfide to 100% sulfate

[a]The densities used in these calculations are:
1.86 g/cm^3 for depths 12'-25' (Parry et al., 1976)

1.94 g/cm^3 for depths 30'-165' (Parry et al., 1976)

2.75 g/cm^3 for depths 175'-200' (Crebs, 1976)

[b]Sill. 1977

[c]Boiling-point surve for liquid water and 0% NaCl.
Taken from Haas, 1971.

Table 14 HEAT FLOW ESTIMATES FROM REACTION ENTHALPIES

Time and Assumptions	Depth-feet		
	200'	2000'	5000'
No oxidation to sulfate Present-day thermal gradient			
.4 m.y.	.02*	.06	.13
.04 m.y.	.23	.64	1.3
.01 m.y.	.93	2.6	5.3
.001 m.y.	9.3	26	53
100% oxidation to sulfate Present-day thermal gradient			
.4 m.y.	.06	.10	.17
.04 m.y.	.61	1.0	1.7
.01 m.y.	2.4	4.0	6.7
.001 m.y.	24	40	67
No oxidation to sulfate Boiling-water thermal gradient			
.4 m.y.	.02	.06	.13
.04 m.y.	.21	.61	1.3
.01 m.y.	.83	2.4	5.1
.001 m.y.	8.3	24	51
100% oxidation to sulfate Boiling-water thermal gradient			
.4 m.y.	.05	.09	.16
.04 m.y.	.46	.86	1.6
.01 m.y.	1.8	3.4	6.0
.001 m.y.	18	34	60

* In heat flow units - $\mu cal/cm^2$ - sec.

Since there are no present day boiling waters, actual temperatures of formation probably lie between these two assumptions. In order to estimate the effect of higher temperatures on these enthalpy calculations, 11 samples were recalculated at these higher temperatures (Table 13).

Calculations were simplified with the following assumptions. Mineral abundances, as determined by computer routine MODECALC, were used. All alunite, K-mica, kaolinite, and montmorillonite formed from feldspars. Where there is very little or no feldspars present, alunite and kaolinite were formed from a 3:2 ratio of plagioclase (assumed pure albite) to orthoclase. This 3:2 ratio is that present at depth in the relatively unaltered quartz monzonite. Where there is significant orthoclase, but less than in weakly altered rock, a 3:1 ratio of albite to orthoclase was assumed for feldspar to kaolinite and alunite reactions. Where orthoclase exceeded that in weakly altered rock, all alunite and kaolinite were formed from albite. No secondary K-spar was assumed. Excess silica was determined by subtracting 66 weight % (average at depth) from the percent SiO_2 of the sample. Because thermodynamic data were not available for opal, precipitation of excess SiO_2 as α-quartz was assumed.

Results

Heat flow estimates resulting from only 200' of alteration or from .001 m.y. of activity are clearly unreasonable. It is doubtful that hydrothermal alteration accounts for more than 50% of the heat flow, as suggested by .001 m.y. A reasonable range of heat flow,

then, is .06 to 6.7 HFU or from .18% to 18% of the total heat flow. The time over which this alteration has occurred clearly exerts the greatest control on heat flow. Depth and intensity of alteration are also very important. If significant fracturing occurs at depth, more intense alteration would probably exist and would increase these heat flow estimates. Since geological and geophysical evidence to date terminate alteration at 500 m (1500 ft) maximum, 2000' is probably the most reasonable, with 5000 ft an over-estimate. Whether there is 0% or 100% of oxidation to sulfate is not very significant with respect to heat flow, since the greater contribution by sulfate is made in the upper 35' (and the next 70' to a lesser extent), which is a small part of the total enthalpy contribution. Though a boiling-water thermal gradient results in somewhat lower heat flows, the difference is not significant.

A solid granitic magma at Roosevelt Hot Springs KGRA cools approximately between the temperatures of 650^{o}C and 283^{o}C (Ward and Sill, 1976). The heat capacity for a typical granite in that temperature range is 97 cal/g or 267 cal/cm^{3}. The advanced argillic zone of alteration produces from 70 - 900 cal/cm^{3}. White (1957) reported that for Steamboat Springs, Nevada, a granitic magma volume of 47 km^{3} would be required to maintain the heat flow of 7 μcal/sec for 100,000 years over a 5km^{2} area. An equal area at Roosevelt Hot Springs, maintaining the 37 HFU for .4 m.y. would require a magma 87 km^{3} in volume.

CONCLUSION

The study of DDH 1-76 identified three alteration zones: Advanced Argillic (quartz + opal + alunite + vermiculite), Argillic (quartz + opal + alunite + kaolinite + muscovite + vermiculite), and Propylitic (quartz + muscovite + montmorillonite + calcite + pyrite and quartz + muscovite + illite-montmorillonite + calcite + chlorite + pyrite).

A simple one-solution geochemical model to explain these alteration assemblages, and remain consistent with measured Roosevelt Hot Springs waters, was not found. Further studies need to resolve the coexistence of opal with muscovite (and not with montmorillonite) in the upper core.

Calculation of reaction enthalpies for all alteration phases resulted in heat flow estimates due to hydrothermal alteration. Although reliable heat flow estimates were difficult due to uncertainty in the extent in time and space over which alteration occurs, hydrothermal alteration can easily account for .2% - 20% of the measured heat flow at DDH 1-76.

APPENDIX 1

XRF Data Reduction Program

```
00101     1*          DIMENSION A(7,8),AA(50,8),B(50,7),SUM(50),XX(50,7)                                000000
00103     2*          DIMENSION Z(50,6)                                                                 000005
00104     3*          DIMENSION DS(7),DNA(7),DLOI(7),WNA(50),WSO3(50),WLOI(50)                          000005
00104     4*    C     A:  MATRIX CORRECTION COEFFICIENTS                                                000005
00104     5*    C     AA:  CALCULATED OXIDE VALUES FROM MULTIPLYING THE ELEMENTAL                       000005
00104     6*    C     ESTIMATES,XX, BY THE MATRIX,A                                                     000005
00104     7*    C     B:  ADDED TO THE A MATRIX AND TAKES INTO ACCOUNT  NA2O,SO3, AND                   000005
00104     8*    C     L.O.I., WHICH ARE DETERMINED SEPARATELY                                           000005
00104     9*    C     SUM:  ADDS ALL OXIDE COMPONENTS FOR A SAMPLE                                      000005
00104    10*    C     XX:  FIRST ESTIMATES OF COMPOSITION                                               000005
00104    11*    C     ZI:  IMPROVEMENTS ON XX                                                           000005
00104    12*    C     DS,DNA,DLOI:  PERCENT SULFUR, SODIUM , AND IGNITION LOSS                          000005
00104    13*    C     WSO3,WNA,WLOI:  NORRISH CORRECTION FACTORS FOR THESE PARAMETERS                   000005
00105    14*          DO 10 N=1,7                                                                       000005
00110    15*          READ (5,300) (A(N,J),J=1,8)                                                       000005
00116    16*          READ (5,375) DS(N),DNA(N),DLOI(N)                                                 000015
00123    17*       10 CONTINUE                                                                          000031
00125    18*          WRITE (6,310)                                                                     000031
00127    19*          WRITE (6,200)                                                                     000036
00127    20*    C     I GOES FROM 1 TO HOWEVER MANY SAMPLES                                             000036
00131    21*          DO 199 I=42,48                                                                    000054
00134    22*          IF (I .EQ. 1) LDEPTH=12                                                           000054
00136    23*          IF (I .GT. 1 .AND. I .LT. 7) LDEPTH=(I+1)*5                                       000062
00140    24*          IF (I .EQ. 7) LDEPTH=38                                                           000104

00142    25*          IF (I .GT. 7 .AND. I .LT. 33) LDEPTH=I*5                                          000112
00144    26*          IF (I .EQ. 33) LDEPTH=162                                                         000133
00146    27*          IF (I .GT. 33) LDEPTH=(I-1)*5                                                     000141
00150    28*          READ (5,202) (XX(I,N), N=1,7)                                                     000152
00156    29*          READ (5,204) WNA(I),WSO3(I),WLOI(I)                                               000163
00163    30*          DO 13 J=1,7                                                                       000176
00166    31*          B(I,J)=(DS(J)*WSO3(I)+DNA(J)*WNA(I)+DLOI(J)*WLOI(I))/100.0                        000176
00167    32*       13 CONTINUE                                                                          000210
00171    33*          KK=3                                                                              000210
00172    34*          SUM(I)=WNA(I)+WSO3(I)                                                             000212
00173    35*          DO 15 JJ=1,7                                                                      000217
00176    36*          SUM(I)=SUM(I)+XX(I,JJ)                                                            000217
00177    37*       15 CONTINUE                                                                          000222
00201    38*          WRITE (6,201) LDEPTH,(XX(I,N),N=1,7),WNA(I),WSO3(I),WLOI(I),SUM(I)                000222
00214    39*          DO 30 N=1,7                                                                       000243
00217    40*          Z(I,N)=XX(I,N)/100.0                                                              000243
00220    41*       30 CONTINUE                                                                          000247
00222    42*       42 DO 60 K=1,7                                                                       000247
00225    43*          AA(I,K)=XX(I,K)+(A(K,1)+A(K,2)*Z(I,1)+A(K,3)*Z(I,2)+A(K,4)*Z(I,3)+                000256
00225    44*         CA(K,5)*Z(I,4)+A(K,6)*Z(I,5)+A(K,7)*Z(I,6)+A(K,8)*Z(I,7)+B(I,K))                   000256
00226    45*       60 CONTINUE                                                                          000306
00230    46*          SUM(I)=WNA(I)+WSO3(I)                                                             000306
00231    47*          DO 154 M=1,7                                                                      000315
00234    48*          SUM(I)=SUM(I)+AA(I,M)                                                             000315
00235    49*      154 CONTINUE                                                                          000320
00237    50*          WRITE(6,201) LDEPTH,(AA(I,MM),MM=1,7),WNA(I),WSO3(I),WLOI(I),SUM(I                000320
00237    51*         C)                                                                                 000320
00252    52*          IF (KK .EQ. 5) GO TO 170                                                          000341
00254    53*          KK=KK+1                                                                           000345
00255    54*          DO 100 K=1,7                                                                      000354
00260    55*          Z(I,K)=AA(I,K)/100.0                                                              000354
00261    56*       100 CONTINUE                                                                         000357
00263    57*          GO TO 42                                                                          000357
00264    58*       170 CONTINUE                                                                         000404
00265    59*       199 CONTINUE                                                                         000404
00267    60*       300 FORMAT (8F8.4)                                                                   000404
00270    61*       310 FORMAT ('205=BCH',3X,'210=AGV',3X,'215=GSP',3X,'220=G-2',3X,'225=S               000404
00270    62*         CARH-1',3X,'230=JB-1',3X,'235=JG-1')                                              000404
00271    63*       200 FORMAT ('LDEPTH',6X,'FE',8X,'TI',8X,'CA',8X,'K',9X,'SI',8X,'AL',8X,'MG',6X      000404
00271    64*         C,'MG',6X,'NA',6X,'SO3',6X,'L.O.I.',6X,'TOTAL')                                   000404
00272    65*       201 FORMAT (1X,I3,6X,11(F6.2,4X))                                                    000404
00273    66*       202 FORMAT (7F5.2)                                                                   000404
00274    67*       204 FORMAT (3F5.2)                                                                   000404
00275    68*       250 FORMAT (I2,F6.4)                                                                 000404
00276    69*       375 FORMAT(3F5.3)                                                                    000404
00277    70*       999 END                                                                              000404
```

APPENDIX 2

Montmorillonite Composition Determination

X-ray diffraction analyses of the three cores of alteration holes drilled by the University of Utah revealed that the 105' depth of DDH 1-A contained the greatest percentage of montmorillonite and was chosen, therefore, as the starting material for analysis.

The sample was crushed to 1/4" size and then pulverized in a tungsten carbide ball mill. This fine grained mixture was then peptized and successively centrifuged to finally separate the -0.2μ size fraction. Considerable enrichment in montmorillonite was achieved. This material was chosen for atomic absorption analysis.

Cation exchange analysis followed standard methods. 200 mg of sample were added to a centrifuge tube with 20 ml 1M ammonium acetate at pH 7. The mixture was shaken 10 minutes and allowed to exchange for one hour. The mixture was centrifuged. The centrate was diluted appropriately and analyzed for Ca, K, Na, Mg. A 100 mg montmorillonite sample was fused in a 1:5 ratio with lithium tetraborate (Spex Industries, Inc., Cat. #6005) according to Brown and others (1969). The resultant bead was dissolved in 10 ml HCl and diluted to 200 ml. This sample was analyzed against appropriate standards (all containing 3 g/l lithium tetraborate, 50 ml/l concentrated HCl, and 1150 ppm Na^+) for Si, Al, Mg, Fe, K, and Ca.

A grey and a green sample were analyzed with the resulting formulas:

grey $(Mg_{.14}Ca_{.08}Na_{.03}K_{.13})(Al_{3.3}Fe_{.19}Mg_{.51})(Al_{.1}Si_{7.9})O_{20}(OH)_4$

green $(Mg_{.14}Ca_{.06}Na_{.01}K_{.06})(Al_{3.27}Fe_{.28}Mg_{.45})(Si_8O_{20})(OH)_4$.

APPENDIX 3

ΔH_f^o and Cp Determination for Vermiculite and Biotite-.6 phlogopite

A magnesium-rich vermiculite has a ΔG_f^o of -1,536,900 calories (Nriagu, 1975). The reaction for the formation of this vermiculite from the elements is written below.

(1) $2.8\,Mg + 0.5Fe + 2.95Si + 1.1Al + 5H_2 + 8O_2 = Mg_{2.8}Fe_{.5}(Si_{2.9}Al_{1.1})O_{10}(OH)_2 \cdot 4H_2O$

The absolute entropy of this vermiculite, S^o, was calculated as suggested by Helgeson (1969) by summing the absolute entropies of the constituent oxides (Table 1, values from Robie and Waldbaum, 1968).

S^o equals 112.0 cal/mole-^oK. For reaction 1, S_r^o was calculated by subtracting the sum of the reactant entropies (Table 1) from the entropy of vermiculite. ΔH_f^o was calculated by:

(2) $$\Delta H_f^o = \Delta G_f^o + T\Delta S_r^o$$

and ΔH_f^o has the value of -1,680,439 calories/mole.

The heat capacity, Cp, of vermiculite was calculated by summing the heat capacity power functions of its constituent oxides (Table 2). Cp vermiculite equals $118.89 + 33.46\times10^{-3}T - 16.29\times10^5\ 1/T^2$.

The heat capacity and ΔH_f^o for biotite (.6 phlogopite) were calculated using equations from Beane (1972). Solve for Cp and ΔH_f^o in equations 3 and 4 using $X_{ann} = .4$ and $X_{phlog} = .6$.

(3) $$C_{Pss} = (100.88X_{ann} + 96.38X_{phlog}) + (37.87X_{ann} + 26.53X_{phlog}) \times10^{-3}T - (5.61X_{ann} + 27.33X_{phlog}) \times10^5T^{-2}$$

(4) $$\Delta^{\circ}H_{fss}^{(298)} = -1{,}299{,}300\ X_{ann} - 1{,}499{,}760\ X_{phlog}$$

The results are:

$$Cp = 98.18 + 31.07 \times 10^{-3}T - 18.58 \times 10^{5}/T^{2}$$

$$\Delta H^{\circ}_{f} = -1{,}391{,}576 \text{ cal/gfw.}$$

Table A3-1

Standard Entropies of Elements and Oxides

Element or Oxide	S°
MgO	6.44
Fe_2O_3	20.89
SiO_2	9.88
Al_2O_3	12.18
H_2O (ice)	10.62
Mg	7.81
Fe	6.52
Si	4.50
Al	6.77
H_2	31.21
O_2	49.00

Table A3-2

Heat Capacity Power Function Coefficients**

Oxide	a	$bx10^{+3}$	$cx10^{-5}$
MgO	10.18	1.74	-1.48
Fe_2O_3	23.49	18.60	-3.55
SiO_2	11.22	8.20	-2.70
Al_2O_3	27.49	2.82	-8.38
H_2O (ice)	9.0	-	-

** Kelley, 1960.

APPENDIX 4

Temperature Measurements for DDH 1-76

Depth-meters	Temperature- C°
5	31.586*
10	42.750
15	58.582
20	65.202
25	70.585
30	78.718
35	85.642
40	90.408
45	95.474
50	98.922
55	102.660
60	107.144
63.5	109.445

* Data taken by Sill, 1977, personal communication.

REFERENCES

Armstrong, R. L., 1970, Geochronology of Tertiary igneous rocks, eastern Basin and Range Province, western Utah, eastern Nevada, and vicinity, U.S.A.: Geochim. et Cosmochim. Acta, vol. 34, p. 203-232.

Ballantyne, J., 1977, personal communication.

Beane, R. E., 1972, A thermodynamic analysis of the effect of solid solution on the hydrothermal stability of biotite: unpublished Ph.D. thesis from the University of Utah, 195 p.

Beane, R. E. 1974, Biotite stability in the porphyry copper environment: Econ. Geology, vol. 69, pp. 241-256.

Best, M. G., Neilson, G. R., and Brimhall, W. H., 1976, X-ray fluorescence analysis of rocks at Brigham Young University, I. Major and minor elements; Communication to W. P. Nash from the Department of Geology at Brigham Young University.

Bowers, D., 1977, Personal communication.

Brown, D. F. G., MacKay, A. M., and Turek, A., 1969, Preparation of stable silica standard solutions in rock analyses using lithium tetraborate: Analytical Chemistry, vol. 41, p. 2091.

Brown, F. H., 1977, Obsidian hydration rinds: geothermal research, Roosevelt Hot Springs Area: Quarterly Progress Report (contract EY-76-07-1601) to ERDA, p. 11.

Brown, F. H., 1977, Attempt at paleomagnetic dating of opal, Roosevelt Hot Springs KGRA: Technical: Vol. 77-1 Report to ERDA (contract EY-76-07-1602), 13 pp.

Browne, P. R. L. and Ellis, A. J., 1970, The Ohaki-Broadlands hydrothermal area, New Zealand: mineralogy and related geochemistry: Am. J. Sci. vol. 269, pp. 97-131.

Butler, B. S., Loughlin, G. F., and Heikes, V. C., 1920, Ore deposits of Utah: U. S. Geol. Survey Prof. Paper 111, 671 pp.

Carr, R. M. and Fyfe, W. S., 1958, Some observations on the crystallization of amorphous silica: Amer. Mineral. vol. 43, pp 908-96.

Crebs, T. J., 1976, Gravity and ground magnetic surveys of the central Mineral Mountains, Utah; Unpub. M.S. thesis, University of Utah, 127 pp.

Criss, C. M., and Cobble, J. W., 1964, The thermodynamic properties of high temperature and aqueous solutions. V The calculation of ionic heat capacities up to 200°, Entropies and heat capacities above 200°: Am. Chem. Soc. Journal v. 86, p. 5390-5393.

Deer, W. A., Howie, R. A., and Zussman, J., 1966, An Introduction to Rock Forming Minerals: Longman Group Ltd., 528 p.

Dedolph, R., and Parry, W. T., 1976, A thermodynamic model of hydrolysis of microcline in acid sulfate solutions: ERDA Grant EY-76-S-07-1601 Technical Report, v. 76-2, Univ. of Utah, 63 pp.

Earll, F. M., 1957, Geology of the central Mineral Range, Beaver County, Utah: unpub. Ph.D. thesis, Univ. of Utah, 112 p.

Evans, S. H., 1977, Mineralogy and petrology of the Mineral Range: Manuscript in preparation.

Garrels, R. M., and Christ, C. L., 1965, Solutions, Minerals, and Equilibria: Freeman, Cooper, and Co., 450 p.

Haas, J. L., Jr., 1971, The effect of salinity on the maximum thermal gradient of a hydrothermal system at hydrostatic pressure: Econ. Geol., v. 66, p. 940-946.

Helgeson, H. C., 1969, Thermodynamics of hydrothermal systems at elevated temperatures and pressures: Am. Jour. Sci., v. 267, p. 729-804.

Hemley, J. J., Hostetler, P. B., Gude, A. J., and Mountjoy, W. T., 1969, Some stability relations of alunite: Ec. Geol., v. 64, pp. 519-612.

Holland, H. D., 1969, Gangue minerals in hydrothermal deposits: Geochemistry of Hydrothermal Ore Deposits (H. L. Barnes, editor); Holt, Reinhart, and Winston, Inc., pp. 382-432.

Honda, S., 1970, Hydrothermal alteration in core from research drill Hole Y-1, Upper Geyser Basin, Yellowstone National Park, Wyoming: Am. Mineralogist, v. 55, p. 1714-1737.

Jacobs, D. C. and Parry, W. T., 1976, A comparison of the geochemistry of biotite from some Basin and Range stocks: Ec. Geol., vol. 71, pp. 1029-1035.

Kelley, K. K., 1960, Contributions to the data on theoretical metallurgy XIII. High-temperature heat-capacity, and entropy data for the elements and inorganic compounds: U.S. Bureau of Mines Bulletin 584, 232 p.

Kharaka, Y. K., and Barnes, I., 1973, Solution-mineral equilibria computations: U.S. Geol. Survey Computer Contribution available from National Technical Information Service, U.S. Department of Commerce, Springfield, Va., 22151, pub. no. 215-899.

Krauskopf, K. B., 1956, Dissolution and precipitation of silica at low Temperatures: Geochemica et Cosmochemica Acta; vol. 10, pp. 1-26.

Lee, W. T., 1908, Water resources of Beaver Valley, Utah: U.S. Geol. Survey Water-Supply Paper 217, 56 p.

Liese, H. C., 1957, Geology of the northern Mineral Range, Millard and Beaver Counties, Utah: unpub. M.S. thesis, Univ. of Utah, 88 p.

Lipman, P. W., Rowley, D. D., Hehnert, H. H., Evans, S. H., Nash, W. P., and Brown, F. H., 1976, Pleistocene rhyolite of the Mineral Mountains, Utah: geothermal and archeological significance: in press, U.S. Geol. Survey Research Bulletin.

Mahon, W. A., and Finlayson, J. B., 1972, The chemistry of the Broadlands geothermal area, New Zealand: Am. J. Sci., v. 272, p. 48-68.

Meyer, C. and Hemley, J., 1959, Hydrothermal Alteration in Some Granodiorites: Clays and Clay Minerals 6th Nat'l Conf., 1957 Proc., pp. 89-100.

Meyer, C. and Hemley, J. J., 1967, Wall Rock Alteration: Geochemistry of Hydrothermal Ore Deposits, ed. H. L. Barnes, pp. 167-235.

Miller, C. D., 1976, Alteration and geochemistry of the Monroe Hot Springs KGRA: unpublished M.S. thesis, University of Utah, 120 pp.

Mundorff, J. C., 1970, Major thermal springs of Utah: Utah Geol. and Mineral Survey Water-Resources Bull. 13, 60 p.

Nash, W. P., 1976, Petrology of the Quaternary volcanics of the Roosevelt KGRA, and the adjoining area, Utah: Final report to National Science Foundation, contract No. GI-43741, vol. 1, 99 pp.

Norrish, K. and Hutton, J. T., 1969, An accurate X-ray spectrographic method for the analysis of a wide range of geologic samples: Geochim, et Cosmochim. Acta, v. 33, no. 4, pp. 431-454.

Nriagu, J. O., 1975, Thermochemical approximations for clay minerals: Am. Mineralogist, v. 60, p. 834-839.

Parry, W. T., Benson, N. L., and Miller, C. D., 1976, Geochemistry and hydrothermal alteration at selected Utah hot springs: Final Report on Grant No. GI-43741, National Science Foundation, vol. 3, 131 pp.

Parry, W. T., Bryant, N. L., and Dedolph, R., 1977, Geochemistry of the Roosevelt Hot Springs Thermal Area, Utah; manuscript in preparation.

Petersen, C. A., 1975, Geology and geothermal potential of the Roosevelt Hot Springs area, Beaver County, Utah: unpub. M.S. thesis, Univ, of Utah, 50 p.

Ransome, F. L., 1909, Geology and ore deposits of Goldfield, Nevada: U.S. Geol. Survey Prof. Paper 66, 258 p.

Raymahashay, B. C., 1968, A Geochemical study of rock alteration by hot springs in the Paint Pot Hill Area, Yellowstone Park: Geochimica et Cosmochimica Acta, v. 32, p. 499.

Robie, R. A., and Waldbaum, D. R., 1968, Thermodynamic properties of minerals and related substances at 298.15°K (25°C) and one atmosphere (1.013 bars) pressure and at higher temperatures: U.S. Geol. Survey Bull. 1259, 256 p.

Schoen, R. and White, D. E., 1965, Hydrothermal alteration in GS-3 and GS-4 drill holes, Main Terrace, Steamboat Springs, Nevada: Econ. Geol., v. 60, p. 1411-1421.

Schoen, R., White, D.E., and Hemley, J. J., 1974, Argillization by descending acid at Steamboat Springs, Nevada: Clays and Clay Minerals, v. 22, p. 1-22.

Sigvaldson, G. E. and White, D. E., 1961, Hydrothermal alteration of rocks in two drill holes at Steamboat Springs, Washoe County, Nevada: Art. 331 in U.S. Geol. Survey Prof. Paper 424-D, pp. D116-D122.

Sigvaldason, G. E. and White, D. E., 1962, Hydrothermal alteration in drill holes GS-5 and GS-7: U.S. Geol. Survey Prof. Paper 450D, pp. D113-D117.

Sill, W. R., 1977, personal communication.

Steiner, A., 1953, Hydrothermal rock alteration at Wairakei, New Zealand: Economic Geology, vol. 48., pp. 1-13.

Swanberg, C. A., 1974, Application of the Na-K-Ca geothermometer to thermal areas of Utah and the Imperial Valley, California: Geothermics, vol. 3, pp. 53-59.

Thompson, G. A. and White, D. E., 1962, Regional geology of the Steamboat Springs Area Washoe County, Nevada: U.S. Geol. Survey Prof. Paper 458-A, pp. A1-A52.

Toulmin, P. and Clark, S. P., 1967, Thermal aspects of ore formation: in Geochemistry of Hydrothermal Ore Deposits, ed. H. L. Barnes; pp. 437-462.

Tripp, A. C., 1977, Electromagnetic and Schlumberger Resistivity Soundings in the Roosevelt Hot Springs KGRA: Unpublished M.S. Thesis, University of Utah, 108 pp.

Ward, S. H., and Sill, W. R., 1976, Dipole-Dipole Resistivity Surveys, Roosevelt Hot Springs KGRA: Final Report, vol 2, to the National Science Foundation, Contract #GI-43741, 42 pp.

White, D. E., 1957, Thermal waters of volcanic origin: Geological Society of America Bulletin; v. 68, pp. 1637-1658.

White, D. E., 1968, Hydrology, activity, and heat flow of the Steamboat Springs thermal system, Washoe County, Nevada: U.S. Geol. Survey Prof. Paper 458-C.

White, D. E., and Muffler, L. J. P., 1964, Metamorphism of upper Cenozoic sediments to greenschist mineral assemblages; Salton Sea Geothermal Area, California: Geol. Soc. America Special Paper 82, Abstracts, pp. 221-222.

White, D. E., Muffler, L. J. P., and Truesdell, A. H., 1971, Vapor-dominated hydrothermal systems compared with hot-water systems: Ec. Geol.; 66, pp. 75-97.